Progress and perspective on polymer templating of multifunctional oxide nanostructures

Xu, Jin; Berg, Alexandra; Noheda, Beatriz; Loos, Katja

Published in:
Journal of Applied Physics

DOI:
10.1063/5.0025052

Journal of Applied Physics

Progress and perspective on polymer templating of multifunctional oxide nanostructures

Cite as: J. Appl. Phys. **128**, 190903 (2020); https://doi.org/10.1063/5.0025052
Submitted: 16 August 2020 . Accepted: 02 November 2020 . Published Online: 20 November 2020

Jin Xu, Alexandra I. Berg, Beatriz Noheda, and Katja Loos

Journal of Applied Physics PERSPECTIVE scitation.org/journal/jap

Progress and perspective on polymer templating of multifunctional oxide nanostructures

Cite as: J. Appl. Phys. **128**, 190903 (2020); doi: 10.1063/5.0025052
Submitted: 16 August 2020 · Accepted: 2 November 2020 ·
Published Online: 20 November 2020

Jin Xu,[1] Alexandra I. Berg,[1,2] Beatriz Noheda,[1,2,a)] and Katja Loos[1,b)]

AFFILIATIONS

[1]Zernike Institute for Advanced Materials, University of Groningen, Nijenborgh 4, 9747 AG, Groningen, The Netherlands
[2]CogniGron Center, University of Groningen, Nijenborgh 4, 9747 AG, Groningen, The Netherlands

[a)]**Author to whom correspondence should be addressed:** b.noheda@rug.nl
[b)]**Electronic mail:** k.u.loos@rug.nl

ABSTRACT

Metal oxides are of much interest in a large number of applications, ranging from microelectronics to catalysis, for which reducing the dimensions to the nanoscale is demanded. For many of these applications, the nano-materials need to be arranged in an orderly fashion on a substrate. A typical approach is patterning thin films using lithography, but in the case of functional oxides, this is restricted to sizes down to about 100 nm due to the structural damage caused at the boundaries of the material during processing having a strong impact on the properties. In addition, for applications in which multifunctional or hybrid materials are requested, as in the case of multiferroic composites, standard top-down methods are inadequate. Here, we evaluate different approaches suitable to obtain large areas of ordered nano-sized structures and nanocomposites, with a particular focus on the literature of multiferroic nanocomposites, and we highlight the polymer-templating method as a promising low-cost alternative.

I. INTRODUCTION

Metal oxides are used in the microelectronics industry as supercapacitors (e.g., ferroelectric oxides such as $BaTiO_3$ or $Ba_{1-x}Sr_xTiO_3$)[1–3] and piezoelectric sensors (e.g., ZnO)[4–6] or for data storage and logic devices.[7] For the latter, memristive oxides (e.g., NbO_x or VO_2), which can switch between various resistance states, are attracting much attention.[8–17] Nanocomposite materials using two different oxides can be desirable to take advantage of the complementary properties of both compounds (e.g., piezo-pyroelectric composites[18]) or in order to achieve large interfacial areas and enhance the coupling of their properties or their connectivities. Despite their promise, fully inorganic nanocomposites are not broadly investigated. More mature in this direction are composites made of ferromagnetic (FM) or ferroelectric (FE) oxides in the so-called multiferroic composites in order to build four-state memories or to increase the magneto-electric coupling arising at the interface of these two components.[19–21] In all these cases, obtaining ordered arrays of the metal oxide on a substrate is preferable.

Often, the synthesis starts with the growth of a thin film of the desired oxide. The main fabrication method for thin film multiferroic nanocomposites is currently pulsed laser deposition (PLD). With PLD, good control over layer thickness can be achieved, and material properties can be tuned through strain engineering, and good quality interfaces can be obtained. However, downsides to this fabrication method are its limitations on large scale production (although this is currently changing[22]), high energy cost, and the need for expensive specialized equipment. Other vapor deposition methods like sputtering and atomic layer deposition (ALD) are also used for the growth of high-quality oxide structures,[23–33] showing better prospects for large area scaling. For the fabrication of nanostructures of metal oxides, thin film deposition alone does not suffice, and a combination with lithography techniques, such as (E) UV-lithography[34,35] and e-beam lithography (EBL),[36–38] or templating, such as anodic aluminum oxide (AAO),[39,40] are required to obtain (complex) nanostructures. In the case of lithography, where dimensions of the structures are diffraction limited, the feature size can be improved greatly by the use of extreme UV (EUV) or electron beam lithography (EBL) instead of standard UV, but these

techniques require highly specialized equipment and come with high energy consumption and costly operation. An alternative way of fabricating thin film nanocomposites and metal oxide nanostructures is through polymer templating. The advantages of this method are its lower cost, its simplicity to pattern, and its simplicity to remove the template.

In this perspective article, we discuss the recent progress of the fabrication of multiferroic thin film heterostructures and functional metal oxide nanostructures through various methods, with a focus on the use of polymer templating and chemical solution deposition (CSD) techniques. We discuss multiferroics as a class of materials for which ordered composites have been reported extensively, with the hope that this perspective will encourage the extension of these methods to other classes of materials (e.g., memristors, ion conductors, piezo-pyroelectric composites, etc.). Section II gives a brief overview of the fabrication of multiferroic nanocomposites through PLD (Sec. II B), the fabrication of templated multiferroic nanostructures using CSD (Sec. II C), and other techniques (Sec. II D). In Sec. III, we focus on the use of polymer templating for the fabrication of functional metal oxide nanostructures. Here, we discuss patterning using block copolymers and the fabrication of nanostructures by common deposition methods such as ALD and CSD, and finally, we discuss other polymer based templating methods.

II. FABRICATION OF MULTIFERROIC THIN FILM HETEROSTRUCTURES

The most intensively studied multiferroic composite geometries are 0–3 heterostructures with magnetic particles (0D) distributed in an FE matrix (3D), 2–2 heterostructures with horizontal (parallel to the substrate) magnetic/FE multilayers (2D), and 1–3 heterostructures with magnetic columns (1D) vertically (perpendicular to the substrate) embedded in an FE matrix (3D), where the two numbers denote the dimension of the corresponding phases, as schematically illustrated in Fig. 1.[41,42]

The first multiferroic composite was fabricated and characterized at Philips. It was a 0–3 $BaTiO_3$–$CoFe_2O_4$ bulk ceramic system fabricated by unidirectional solidification of a eutectic quinary Fe–Co–Ti–Ba–O system.[43,44] An ME coefficient, α_E, as high as 50 mV/cm Oe was observed. Later on, co-sintering became the most popular technique in the preparation of ceramic 0–3 bulk composites.[45–47] Techniques such as hot pressing,[48] spark plasma sintering,[49] and aerosol deposition[50] were later introduced to improve the quality of the FE/FM interface by reducing the sintering temperature. Solgel processing[51,52] was also used to achieve a better distribution of the FM particles. Another way to improve the distribution is to cast a solution of ferroelectric poly (vinylidene fluoride-co-trifluoroethylene) [P(VDF-TrFE)] containing well-dispersed ferroic nanoparticles.[53–56] Preparation methods for 2–2 bulk composites include co-firing of the constituent phases,[57] tape casting of alternating layers of FE and FM phases,[58,59] and epoxy bonding of FE and FM sheets.[60,61] A very few 1–3 bulk composites were reported. One of the few examples is the dice-and-fill technique, where a diced PZT pellet was filled with Terfenol-D particles dispersed in an epoxy resin solution.[62]

A. Fabrication of 0–3 and 2–2 multiferroic thin film heterostructures

The continuous miniaturization of devices has made the compatibility of multiferroics to integrated circuits crucial, especially for their use in memory devices. This renders thin film composites advantageous over bulk composites, owing to their smaller volume, lower operating voltage, and thus lower power consumption.

Not much work has been done on the fabrication of 0–3 thin-film heterostructures. The solgel process is the main method used, in which the composites were crystallized from a spin-coated thin film of either a precursor of the FE phase containing FM nanoparticles[63,64] or a mixture of the FE precursor and FM precursor.[65–69] The self-assembly of spinel ferromagnets and perovskite ferroelectrics during pulsed laser deposition (PLD) can also result in a 0–3 geometry, according to the work of Ryu *et al.*[70] The main issue for the 0–3 heterostructure is the large leakage current caused by percolation (most ferromagnets are conductive), which makes the distribution of the FM particles crucial to the properties.

Compared to the 0–3 geometry, the 2–2 layered multiferroic thin films are much easier to deposit and suffer much less leakage, thanks to the good insulation by the FE layers. Many systems such as bilayers,[71–77] multilayers,[68,78–81] FM thin films on single crystalline FE substrates[82–86] and FE thin films on magnetic substrates[87,88]

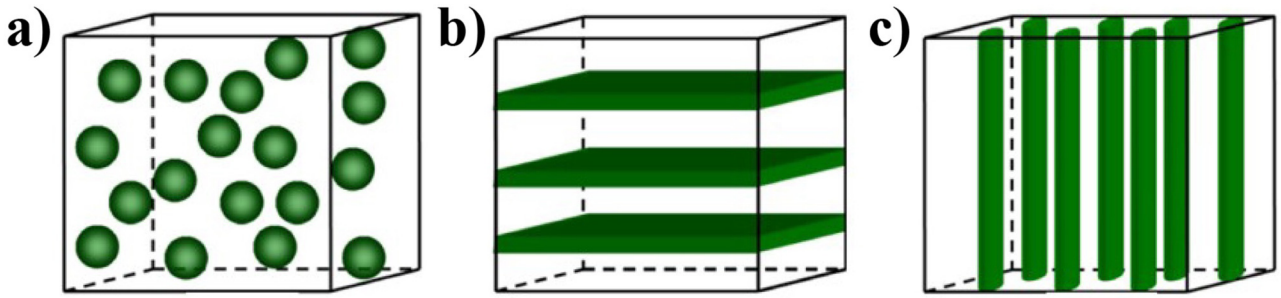

FIG. 1. Schematic illustration of the three most studied multiferroic heterostructures: (a) 0–3 heterostructure consisting of magnetic particles embedded in the FE matrix, (b) 2–2 heterostructure of horizontal magnetic-FE bilayers or multilayers, and (c) 1–3 heterostructure consisting of vertical magnetic columns embedded in an FE matrix. Reprinted with permission from Nan *et al.*, J. Appl. Phys. **103**, 031101 (2008). Copyright 2008 AIP Publishing LLC.

have been investigated. PLD and chemical solution deposition (CSD), for example: solgel process and metallo-organic decomposition, were used predominately, in which PLD typically results in epitaxial films,[71,72,89,90] whereas CSD normally results in polycrystalline films.[78,91] Many 2–2 multiferroic thin films exhibit magnetoelectric (ME) coefficients comparable to their corresponding bulk systems.[41]

B. Pulsed laser deposition of multiferroic 1–3 thin film heterostructures

Nan *et al.*[92] theoretically predicted a much stronger magnetic-field-induced electric polarization (MIEP) in 1–3 multiferroic thin films than in 2–2 multiferroic thin films. This is a result of less in-plane mechanical constraint from the substrate, thus less inhibition of magnetostriction. These 1–3 systems also provide a larger interface area than 2–2 systems, which is in favor of coupling strength as well.

In 2004, a novel approach to heteroepitaxial 1–3 spinel-perovskite nanocomposites was presented by Zheng *et al.*[93] In this approach, columns of ferromagnetic insulating $CoFe_2O_4$ embedded in a ferroelectric $BaTiO_3$ matrix were formed by self-assembly during PLD, as shown in Fig. 2. It soon became the prototype synthesis method of 1–3 spinel-perovskite nanocomposites. Not only $CoFe_2O_4$–$BaTiO_3$,[94,95] but also a variety of other composite thin films such as $CoFe_2O_4$–$BiFeO_3$,[96–101] $CoFe_2O_4$–$PbTiO_3$,[102–106] $NiFe_2O_4$–$BiFeO_3$,[96,107] $BiFeO_3$–$MgFe_2O_4$,[108] $Sr(Ti_{1-x}Fe_x)O_3$–$CoFe_2O_4$,[109] and $CoFe_2O_4$–$Bi_5Ti_3FeO_{15}$[110] were deposited. Different sets of parameters like substrate orientation, phase composition, and growth rate lead to rich morphologies such as embedded rods, embedded triangles, labyrinth-like morphology, lamellar-like morphology, etc.[97,101,102,107,109,111,112]

The size and position of $CoFe_2O_4$ (CFO) nanopillars formed in the self-assembly process are not defined. To improve the regularity, various patterning techniques have been utilized. For example, Comes *et al.*[38] created a layer of highly ordered CFO arrays by ion etching through an electron-beam-lithography (EBL)-defined etching mask. A small amount of $BiFeO_3$ (BFO) was then filled in between the CFO pillars to form a seed layer. The co-deposition of BFO and CFO was subsequently performed. The fabrication procedure is schematically illustrated in Figs. 3(a)–3(f). AFM images of the CFO nanoarrays and the nanocomposite are shown in Figs. 3(g) and 3(h), respectively. Besides etching masks, stencil masks made from anodic aluminum oxide (AAO) membranes[39,40] have also been used for the seed layer creation.

Another way of generating seed layers was developed by the group of Ross. The principle is to selectively nucleate CFO or other spinel ferromagnet islands inside highly ordered pits on the substrate. This is feasible due to the high diffusion rate during slow PLD and post-deposition annealing. The substrate patterning methods reported by the Ross group include focused ion beam (FIB) etching followed by an acid treatment[113,114] and wet etching through porous block-terpolymer template.[115] The procedure of composite growth on FIB-etched substrates is schematically illustrated in the upper part of Fig. 4. The lower part of Fig. 4 shows the morphology at each preparation step. We refer the readers to the recent work of the group of Ross for an extensive overview of epitaxially grown thin film perovskite-spinel nanocomposites and their integration on silicon.[116]

C. Chemical solution deposition of multiferroic 1–3 thin film heterostructures

Although being the dominant fabrication technique for 1–3 thin film heterostructures, PLD has many limitations on large scale production. It requires expensive and specialized equipment and consumes a considerably large amount of energy. In addition, the templating methods described above rely on the very different surface energies of the different constituents in order to achieve selective growth, limiting the composites to combinations of spinel (AB_2O_4) and perovskite (ABO_3). In comparison, chemical solution deposition (CSD) is much cheaper, more energy-efficient, more suitable for large samples, and not limited to the spinel and

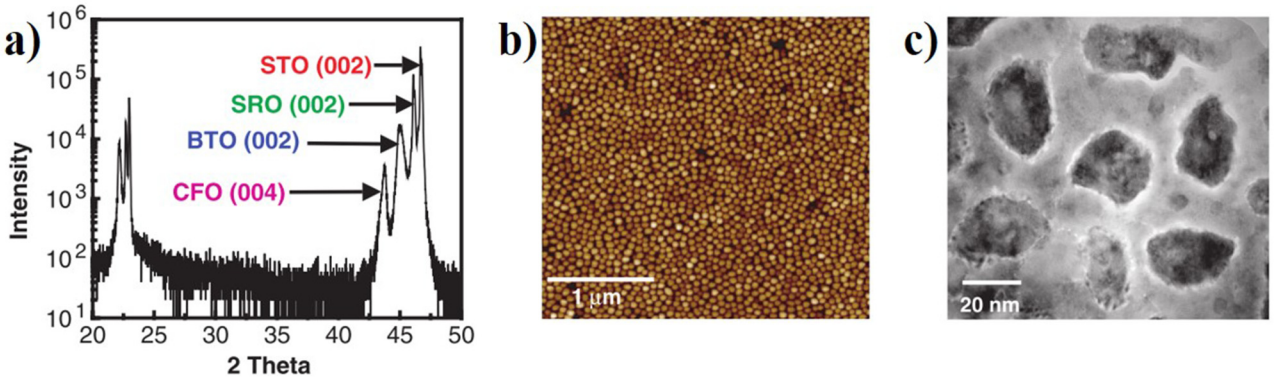

FIG. 2. (a) X-ray diffraction (XRD) spectrum of the self-assembled $CoFe_2O_4$-$BaTiO_3$ (CFO-BTO) composite on the $SrRuO_3$-covered $SrTiO_3$ (SRO-STO) substrate. The (00l) peaks of the CFO, SRO, and STO indicate an epitaxial relationship between the layers. (b) Atomic force microscopy (AFM) height image of the composite film. (c) Planar-view transmission electron microscopy (TEM) image, where the dark columns are CFO and the brighter matrix is BTO. Reprinted with permission from Zheng *et al.*, Science **303**, 661 (2004). Copyright 2004 AAAS.

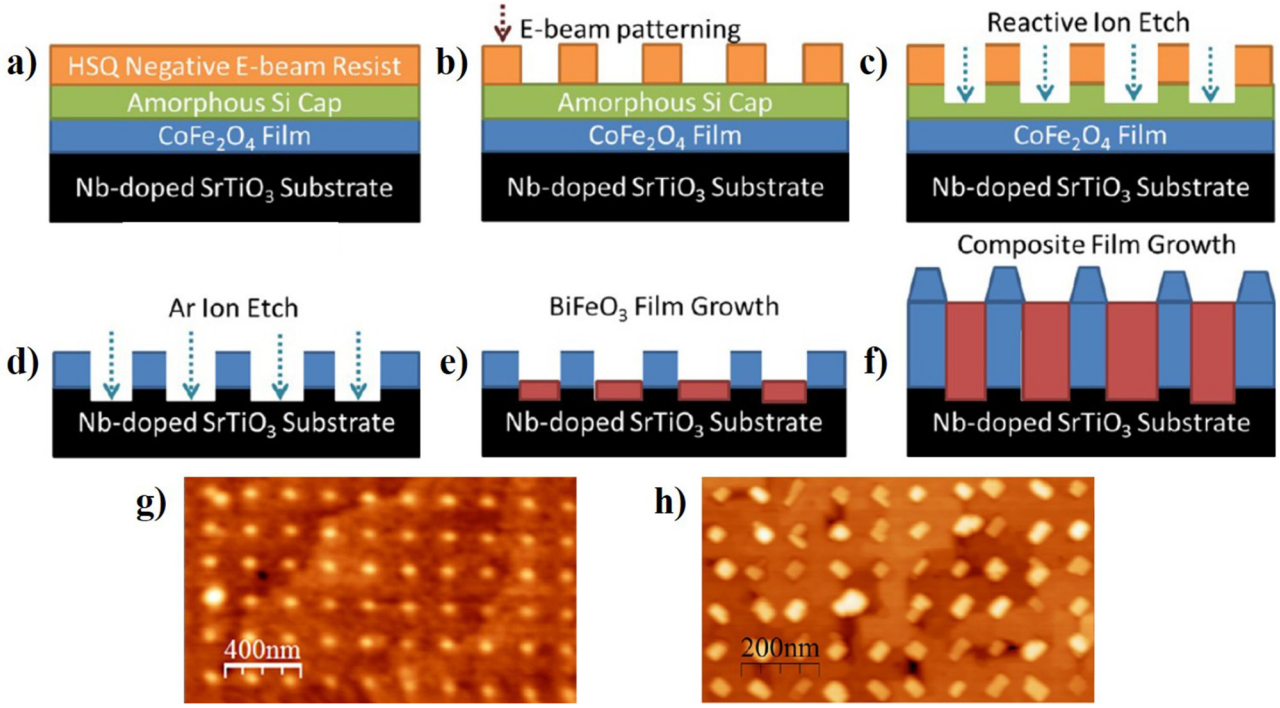

FIG. 3. (a)–(f) Schematic illustration of the deposition steps of highly ordered $CoFe_2O_4$–$BiFeO_3$ nanocomposites. AFM images of (g) CFO nanoarrays and (h) the as-fabricated nanocomposite. Reprinted with permission from Comes *et al.*, Nano Lett. **12**, 2367 (2012). Copyright 2012 American Chemical Society.

perovskite material combination. Yet, a very few attempts have been made on CSD of 1–3 multiferroic thin film heterostructures. Luo *et al.*[117] prepared an epitaxial $BaTiO_3$–$NiFe_2O_4$ (BTO–NFO) nanocomposite thin film on $LaAlO_3$ substrates via spin coating and thermal annealing of an aqueous solution containing polymer-bound Ba, Ti, Ni, and Fe ions. Phase separation between BTO and NFO occurred during annealing, resulting in a composite of NFO nano-grains embedded in a BTO matrix. Liu *et al.*[118] synthesized an epitaxial BTO–CFO 1–3 system on an $SrTiO_3$ (STO) substrate via a solgel process. A sol containing diethanolamine-stabilized Bi, Ti, Co, and Fe cations was spin-coated and annealed. The resulting nanocomposite was again formed via self-assembly. Cross-sectional TEM images and energy dispersive spectrum (EDS) analysis of the nanocomposite are shown in Fig. 5.

Ren *et al.*[119] made an attempt to direct the self-assembly of FE and FM phases during CSD. Amphiphilic block copolymer polystyrene-block-poly (ethylene oxide) (PS-b-PEO) was added to the precursor solution containing Pb, Zr, Ti, Co, and Fe cations. After spin-coating and solvent vapor annealing, the two polymer blocks formed quasi-hexagonal packed micelles [Fig. 6(a)]. Oxidation and crystallization during thermal annealing yield a polycrystalline 1–3 heterostructure with CFO cylinders embedded in a $Pb_{1.1}Zr_{0.53}Ti_{0.47}O_3$ (PZT) matrix [Figs. 6(b) and 6(c)].

Although high-quality 1–3 nanocomposite thin films can be obtained via CSD, the self-assembly from mixed solutions still results in poorly defined structures. Besides, no thorough studies on the multiferroic and magnetoelectric properties were reported on the CSD-defined composites.

D. Other thin film heterostructures

In addition to the conventional 0–3, 2–2, and 1–3 systems, a range of other types of thin film heterostructures have been created, for instance, FM nanostructures grown on FE single crystalline substrates. Kim *et al.*[120] placed Ni nanocrystals on top of a highly piezoelectric ferroelectric $(PbMg_{1/3}Nb_{2/3}O_3)_{1-x}$:$(PbTiO_3)_x$ (PMN–PT, $x \approx 0.32$) single crystalline substrate by solution casting. A difference in magnetic hysteresis and blocking temperature was noticed before and after electric poling of the FE substrate, demonstrating a coupling between Ni and PMN–PT. Sohn *et al.*[121] created Ni rings on top of a PMN-PT substrate, via Ni evaporation and lift-off on an EBL-patterned photoresist layer. The domain walls in the Ni rings could be tuned by an applied electric field, indicating ME coupling.

Another example of an unconventional thin film heterostructure is the core–shell nanostructure. Pan *et al.*[36] fabricated arrays of CFO-PZT core–shell cylinders through a so-called soft-EBL approach. In this approach, arrays of pores were created by solvent development of EBL-patterned double resist layers. The exposed substrate inside the pores was functionalized with small molecules, which prevents sol attachment to the substrate during the next PZT sol deposition. As a result, the spin-coated PZT sol only attaches to

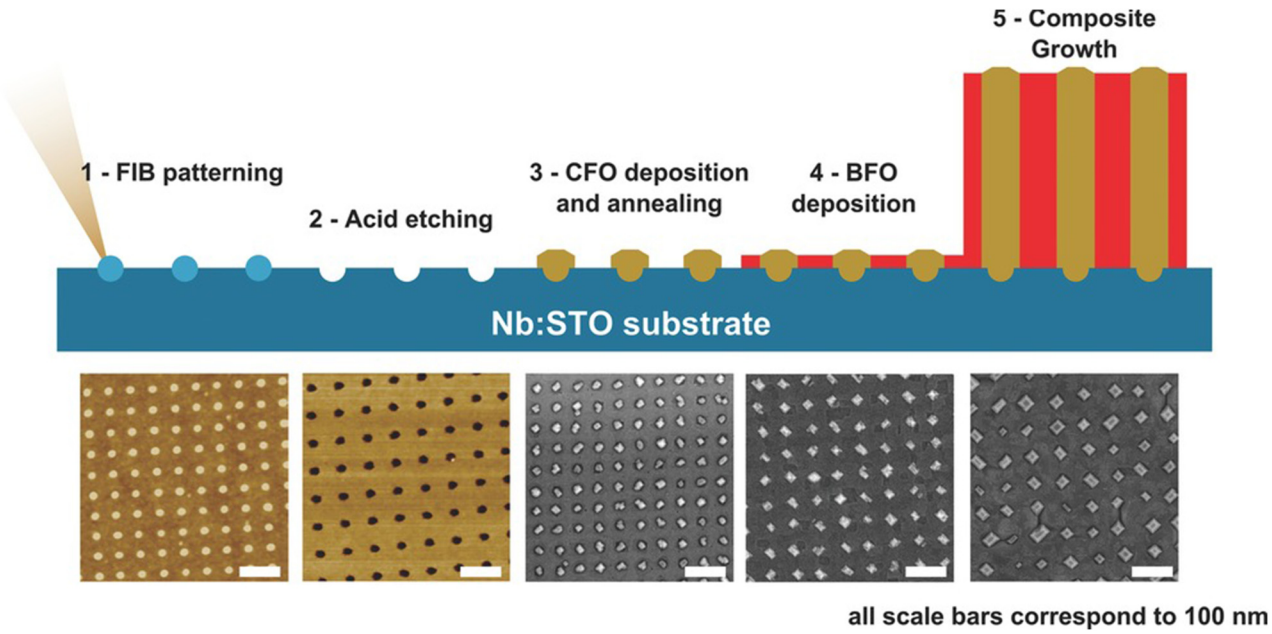

FIG. 4. Schematic illustration of the procedure of $CoFe_2O_4$-$BiFeO_3$ (CFO-BFO) nanocomposite fabrication. A CFO seed layer is created by selective nucleation in FIB-defined pits in the substrate. The images below the flow chart are the sample morphology at the corresponding preparation stage (1–5). From left to right, these are: AFM image of the FIB patterned Nb:STO substrate; AFM image of the substrate after acid etching; scanning electron microscopy (SEM) image of the CFO arrays; SEM image of the CFO-BFO seed layer and SEM image of the final composite. Reprinted with permission from Aimon *et al.*, Adv. Mater. **26**, 3063 (2014). Copyright 2014 Wiley-VCH.

the walls of the bottom resist layer, forming shells of the core–shell structure after drying. The subsequently deposited CFO sol after removing the surface functionalization becomes the core of the core–shell structure. Lift-off and thermal treatment in the last step removes the remaining resist and oxidizes the sols, respectively. A schematic illustration of the fabrication process and the resulting structure is depicted in Figs. 7(a) and 7(b), respectively. Lu *et al.*[40] reported a similar core–shell structure of a CFO–BFO system, fabricated by PLD through an AAO stencil mask. The core–shell arrangement is a result of self-assembly under controlled confinement of the mask.

A 0–0 heterostructure was proposed by Lu *et al.*,[122] in which FM and FE materials were stacked layer by layer within pillars. Compared to the conventional 2–2 heterostructures, such a design promises better control on the size and thickness of FM and FE phases, larger flexibility on material design (number of layers,

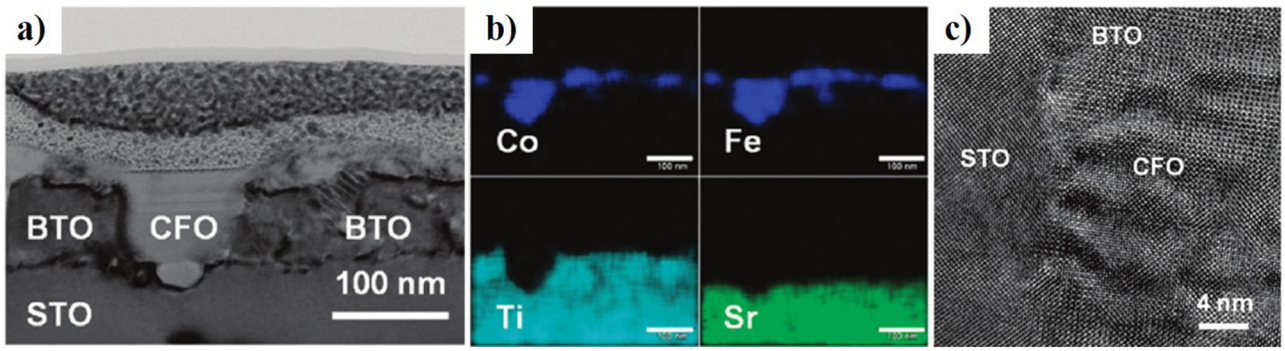

FIG. 5. (a) Cross-sectional bright-field TEM image of a solgel derived BTO–CFO thin film on the STO substrate, (b) energy dispersive spectrum (EDS) element mapping (scale bar 100 nm) of the area in (a). (c) High-resolution cross-sectional TEM image showing the STO-CFO-BTO interface, indicating an epitaxial relationship. Adapted with permission from Liu *et al.*, ACS Nano **4**, 6836 (2010). Copyright 2010 American Chemical Society.

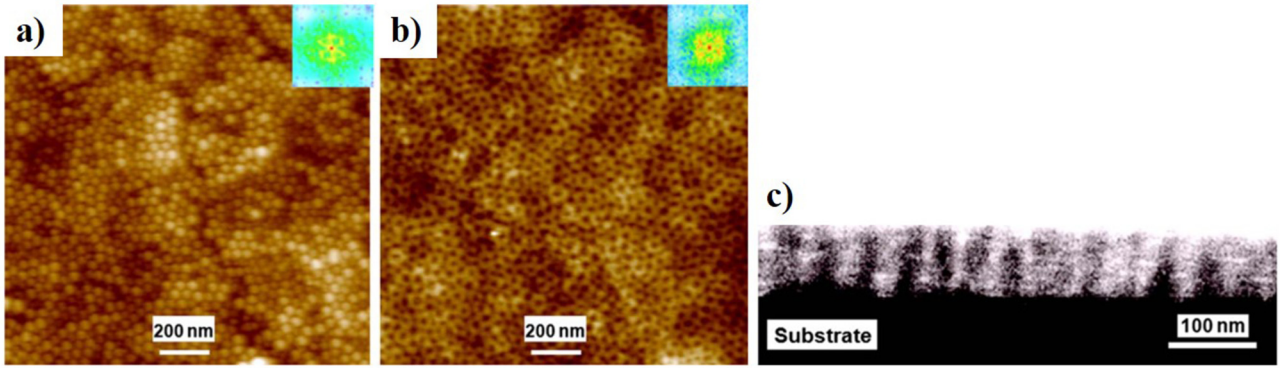

FIG. 6. AFM images of (a) thin film containing PS-b-PEO and metal cations after solvent vapor annealing and (b) film in (a) after thermal treatment. The insets are the fast Fourier transforms of the corresponding images. (c) Cross-sectional TEM image of the nanocomposite, confirming a 1–3 structure. Adapted with permission from Ren *et al.*, Appl. Phys. Lett. **93**, 173507 (2008). Copyright 2008 AIP Publishing LLC.

stacking sequence, etc.), and reduced clamping effect. The preparation was done via layer-by-layer PLD through an AAO stencil mask. The same method was utilized by Tian *et al.*[123] in the preparation of $SrRuO_3$–$CoFe_2O_4$–$BiFeO_3$ (SRO–CFO–BFO) triple-layer 0–0 heterostructures, where SRO was the top electrode. A schematic description of the preparation steps can be found in Fig. 8(a). The morphology obtained is illustrated by SEM and cross-sectional TEM in Figs. 8(b)–8(d), respectively. The XRD spectrum in Fig. 8(c) reveals an epitaxial nature of the stacks.

The disk-matrix structure of ordered arrays of FM nanodisks embedded in the FE matrix is another type of unconventional multiferroic heterostructure. It can be considered as a special type of 1–3 heterostructure with low aspect ratio FM pillars. FM nanodisks are created prior to the deposition of the FE film, usually via guided PLD through AAO stencil masks[124] or Si_3N_4 stencil masks.[125] Multilayers of these disk-matrix thin films can be obtained by repeating the process, making it more similar to the 0–3 type heterostructure. Cross-sectional TEM images of a CFO–PZT and a NFO–PZT disk-matrix nanocomposite fabricated with stencil masks are depicted in Figs. 9(a) and 9(b), respectively.

III. POLYMER THIN FILMS AS TEMPLATES FOR METAL OXIDE NANOSTRUCTURES

As demonstrated in Sec. II C, the self-assembly of a mixed precursor solution of FM and FE oxides typically yields poorly

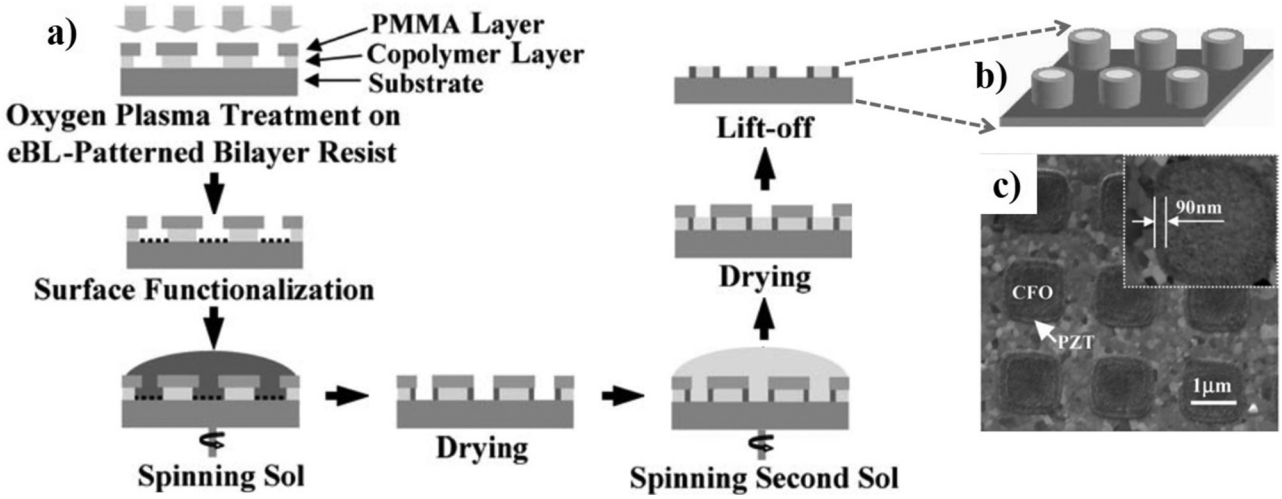

FIG. 7. (a) Soft EBL preparation process of CFO-PZT core–shell nanocomposites, where the first and second sols are PZT sol and CFO sol, respectively. (b) Schematic illustration of the final composite structure. (c) SEM backscattered-electron image of the obtained nanocomposite. Adapted with permission from Pan *et al.*, Small **2**, 274 (2006). Copyright 2006 Wiley-VCH.

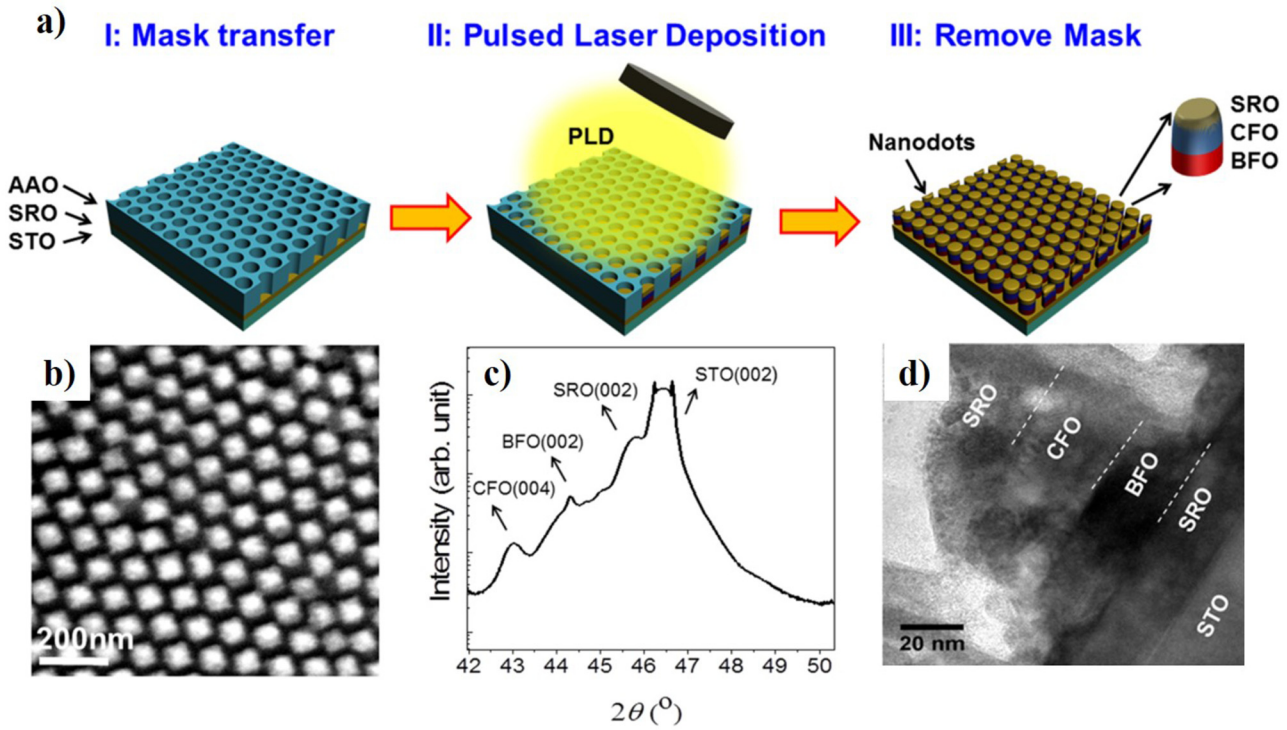

FIG. 8. (a) Schematic illustration of the fabrication process of CFO-BFO 0–0 heterostructure. (b) SEM image of the obtained nanostructure. (c) XRD spectrum of the pillars, revealing an epitaxial growth quality. (d) Cross-sectional TEM image of one pillar. Adapted with permission from Tian *et al.*, ACS Nano **10**, 1025 (2016). Copyright 2016 American Chemical Society.

defined ordering and interfaces. To enable the alternative deposition methods such as ALD and CSD in the fabrication of well-defined 1–3 or dot-matrix multiferroic heterostructures, the patterning of the FM oxide phase prior to the FE phase deposition is required. The fabrication of an ordered array of nanodisks covered with a thin FE film (Sec. II D, Fig. 9) could be seen as a basis for a two-step fabrication method of (1–3) MF nanocomposites. So far, not a lot of work has been done on such two-step fabrication, but there are opportunities in this method with advantages over the conventional PLD methods, especially with the use of polymer templates.

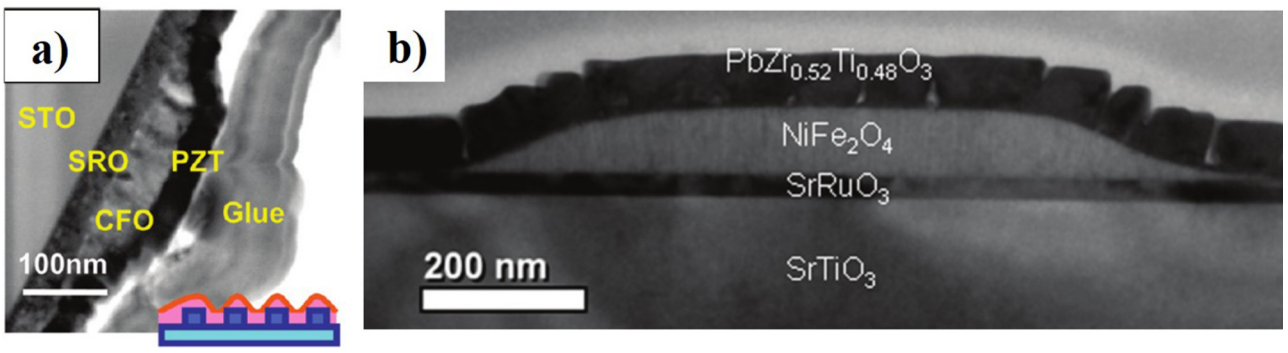

FIG. 9. Cross-sectional TEM images of (a) a single CFO disk covered by a PZT film. Reprinted with permission from Gao *et al.*, ACS Nano **4**, 1099 (2010). Copyright (2010) American Chemical Society. (b) An NFO nanodisk covered by a PZT thin film. Reprinted with permission from Vrejoiu *et al.*, Nano Rev. **2**, 7364 (2011). Copyright 2011 Taylor & Francis Ltd.

AAO membranes[126,127] and silica colloidal crystal monolayers[128,129] have both been utilized as templates in CSD or ALD growth of oxides. However, both methods suffer difficulties on complete removal after deposition. Mechanical removal of the AAO membrane leaves pieces in the sample, while acid or basic etching may damage the oxide nanostructure. For silica colloid templates, wet etching removal has the same problem. On the contrary, polymer-based templates vanish completely after pyrolysis or dissolution with solvents, leaving cleaner nanostructures.

Block copolymers (BCPs) are popular polymer templates for nanopatterning. Main advantages are the low cost, ease of fabrication, and suitability to large-area deposition. Additionally, BCP templating is highly versatile due to the tunability of the polymer blocks, allowing for different structures and dimensions of the templated material. Although a few examples can be found on oxide templating with thin films of BCP micelles,[130–135] most BCP templating processes require BCP microphase separation and self-assembly, to obtain highly ordered BCP nanostructures. This microphase separation is a result of unfavorable interaction between the polymer blocks: the immiscibility drives polymer blocks to phase separate, and the covalent linkage between them prevents them from macrophase separation. The equilibrium nanostructure of a BCP melt depends on the total length of the BCP, the volume ratio of the two blocks, and the strength of interaction between the two blocks, as revealed by the mean-field phase diagram (Fig. 10),[136] thereby leading to self-assembly into different morphologies.[137–142]

Self-assembly in BCP thin films is more complicated. Parameters like film thickness, substrate interaction with each block, and free surface selectivity can influence the morphology significantly.[140] For the purpose of oxide patterning, vertical lamellae and vertical cylinders are most desirable. However, for applications in which coupling between different materials is not the key feature but, for example, percolation is (e.g., memristors) other geometries are also interesting. Pushing the lamellae and cylinders to stand up can be achieved in several ways, of which the most common are the application of an electric or magnetic field across the film thickness,[143,144] creating a neutral substrate surface with chemical modification,[145] or solvent vapor annealing (SVA), which is the simplest and most broadly applied method.

During deposition, the BCP thin film provides a template, the structure of which will determine the suitable deposition methods. If the template is porous, any low temperature deposition technique can be used. However, when the template is not porous, a loading technique is required. For the templating of oxides, one of the polymer blocks serves as the host for metal-precursor molecules (gas or liquid phase), allowing for bottom-up growth of the metal oxide inside one of the polymer blocks according to the template of the BCP. A thermal annealing or plasma cleaning step results in the removal of the organic matrix, leaving only the inorganic metal oxide nanostructures. This method is highly versatile and tunable and has received attention over the past years, starting with the fabrication of metallic nanostructures[146,147] to the fabrication of functional metal oxides, with possible applications in data storage (multiferroic nanocomposites),[116] adaptable electronics (memristors, conductive networks),[148] and optoelectronics.[149] This templating technique can also be used to fabricate organic–inorganic composites, where inorganic nanoparticles are included in a BCP matrix. BCP templates can act as etching masks for oxide layers underneath[150] or as shadow masks or guides for vapor deposition techniques such as PLD[151–153] and atomic layer deposition (ALD).[149,154–159]

Below, we evaluate two of the most common oxide deposition methods for block copolymer templating: sequential infiltration synthesis (SIS, Sec. III A) and chemical solution deposition (CSD, Sec. III B). Finally, we discuss some other polymer-based templating methods in Sec. III C.

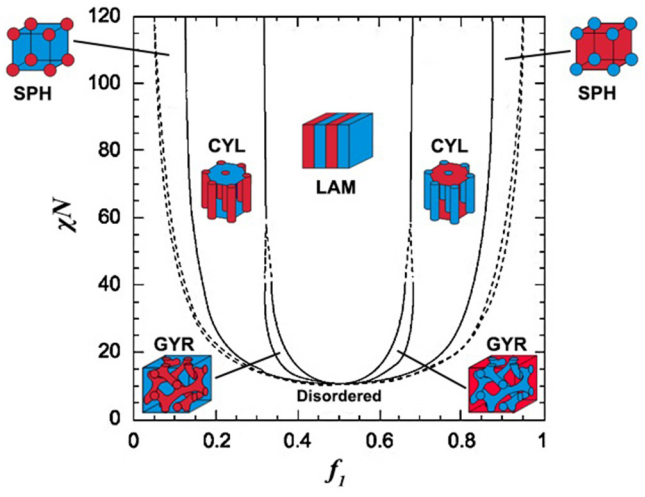

FIG. 10. Theoretical phase diagram of diblock copolymer melts calculated by the mean-field theory, where χ is the interaction parameter of the two blocks, N is the total number of segments in the block copolymer, f_A is the volume fraction of block A (red block in the picture). The possible phases are denoted as SPH (spherical), CYL (cylindrical), LAM (lamellar), GYR (gyroid), and DIS (disordered). Reprinted with permission from Hofman *et al.*, Polymer **107**, 343 (2016). Copyright 2016 Elsevier.[215]

A. Block copolymer templating using sequential infiltration synthesis

One of the main deposition techniques for block copolymer templating is sequential infiltration synthesis (SIS). This technique is based on ALD, sharing the same equipment and chemical precursors, and allows for controlled, self-limited growth of metal-organic precursors in (block co)polymers. Therefore, SIS is not as low-cost as CSD-based techniques, since the equipment and precursors are costly. However, ALD is widely used in industries, allowing for large-area, low-temperature growth, making ALD-based SIS a relevant technique to review in the context of this work. SIS differs from ALD in the process parameters: higher pulse pressure of precursors to provide enough precursors to infiltrate the polymer matrix (3D volume) and longer exposure times to allow for complete diffusion into the polymer film (Fig. 11).[157,160] Horizontal BCP morphologies are more common in SIS compared to CSD, most likely due to the ability of the vapor phase precursors to diffuse into the polymer matrix. This method was first described

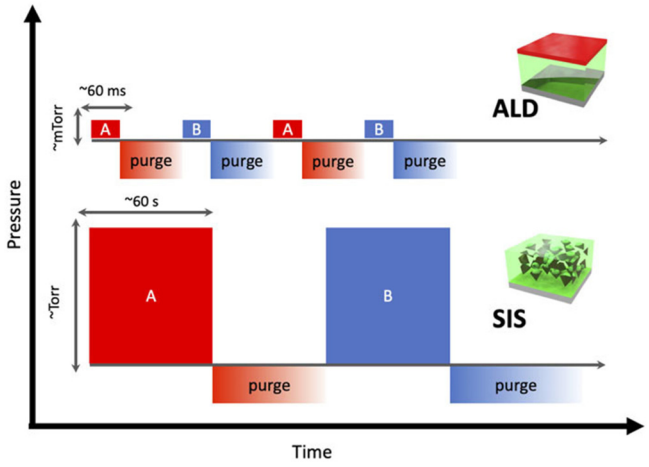

FIG. 11. Comparison between process parameters of atomic layer deposition (ALD, top) and sequential infiltration synthesis (SIS, bottom). The pulse pressure and duration are short for ALD, whereas the pressure and pulse duration are much higher for SIS to allow for high enough concentration of precursors to infiltrate and completely diffuse through the polymer matrix. Reprinted with permission from Waldman *et al.*, J. Chem. Phys. **151**, 190901 (2019). Copyright 2019 AIP Publishing LLC.

by Peng *et al.*[157,161] as a way to selectively grow metal oxides in one domain of a BCP and control the growth at a molecular level. SIS is based on two key steps: the selective and self-limited interaction of the metal precursors in the gas phase with the BCP template. The selectivity of the reaction is based on Lewis acid–base interactions of the organometallic precursors (Lewis acids) with the functional groups in one of the blocks of the BCP (Lewis bases). Due to these specific reaction sites in the polymer template, the reactions are self-limited and heterogeneous, this allows for controllability at the molecular level. Excess unreacted precursors are purged after each growth cycle to ensure that the reactions are indeed self-limited and heterogeneous.[157,160–162] For an interesting perspective on the thermodynamics and kinetics of SIS, we refer the reader to Waldman *et al.*[160]

Peng *et al.*[157] first demonstrated the growth of Al_2O_3 and TiO_2 cylinders in PS-*b*-PMMA. The organometallic precursors react with the carbonyl groups of PMMA to generate reaction sites for subsequent growth cycles, whereas the PS domains are inert for the reaction, leading to selective infiltration of the PMMA domain. The dimensions of the metal oxide nanostructures could be tuned by varying the total number of growth cycles. In a follow-up paper in 2011, they presented a strategy to employ SIS with PS-b-PMMA for materials that otherwise would not grow in the PMMA block, such as ZnO, SiO_2, and W.[161] Using trimethyl aluminum (TMA), the PMMA block is selectively modified during the first SIS cycle by reacting with the carbonyl groups, generating reactive –Al–CH_3/–Al–OH sites that can seed the growth of other materials. In 2019, Azoulay *et al.*[163] even reported the growth of cylindrical ZnO/Al_2O_3 heterostructures in PS-*b*-PMMA in one SIS process, using the principle of priming the PMMA block with AlO_x to allow for the growth of ZnO. Heterostructures could be formed since the zinc precursor (diethylzinc, DEZ) penetrates deeper into the polymer matrix than TMA, resulting in cylinders of ZnO capped with Al_2O_3 (Fig. 12). While the growth of Al_2O_3 using TMA and H_2O (oxidizing agent) in PS-*b*-PMMA has become a model system for studying SIS, many different materials have been grown using PS-*b*-PMMA and other polymer templates: Al_2O_3,[157,158,164–168] ZnO,[149,158,161,163,165,166] TiO_2,[157,158,165] SiO_2,[161] Ga_2O_3,[169] In_2O_3,[169] SnO_2,[159] VOx,[158] W/WO_x.[161]

Some advances in SIS since the introduction of the method are discussed below. In 2013, Kamcev *et al.*[165] demonstrated the growth of ZnO, TiO_2, and Al_2O_3 in the PS block of PS-*b*-PMMA through a chemical modification by UV exposure of the polymer film. Photo-oxidation by the UV light leads to the breakdown of the phenyl groups of PS to the Lewis basic hydroxyl, carboxyl, carbonate, and carbonyl groups. Each of these groups has increased Lewis basicity compared to PMMA, enabling the block-selective growth in the PS domain. Frascaroli *et al.*[167] were the first to use O_3 as an oxygen precursor in SIS, instead of H_2O, to improve reaction conditions during growth. The disadvantages of the use of water are low growth rates at low temperatures and difficulty of purging from the chamber, leading to long processing and purging times. Ozone has a higher reactivity than H_2O, leading to faster growth rates at low temperatures, and it is much easier to purge, reducing the overall process time of SIS. They also found reduced hydrogen contamination in the final metal oxides when using O_3 as an oxygen precursor, this is mostly interesting for electrical applications. Recently, Subramanian *et al.*[149] reported the fabrication of a 3D nanomesh of ZnO for optoelectronic applications, the first demonstration of optoelectronic device functionality of a nanostructure based on BCP templating and SIS. They used lamellar morphology PS-*b*-P2VP, the pyridine moiety in P2VP has a higher chemical reactivity compared to PMMA, allowing for a more favorable interaction with the zinc precursor. This removes the need to prime the BCP with insulating AlO_x for the growth of ZnO, which is favorable for the electrical properties of the material. Additionally, they report a modification of the SIS protocol: micro-dose infiltration synthesis (MDIS). In MDIS, the precursor is pulsed multiple times, with set intervals, during the exposure period, this increases the precursor concentration in the reaction chamber (Fig. 13). The higher concentration leads to a higher uptake of the precursors into the polymer matrix with each growth cycle. MDIS resulted in a more uniform incorporation of the precursor in the BCP matrix compared to the standard SIS. For an extensive review on SIS on polymer-based templates and applications of infiltration-designed materials, we refer the reader to Berman *et al.*[162]

B. Block copolymer templating using chemical solution deposition

The second main deposition technique for BCP templating is CSD. A typical route of block copolymer templating using CSD was developed by the group of Morris[140,143,145,152,170–173] for oxide nanodots. Highly ordered arrays of Ce_2O_3, Fe_3O_4, Fe_2O_3, and PZT nanodots were obtained from polystyrene-*block*-polyethylene oxide (PS-*b*-PEO) templates. Thin films of hexagonally packed PEO cylinders in the PS matrix [Figs. 14(a), 14(a1), and 14(a2)] were

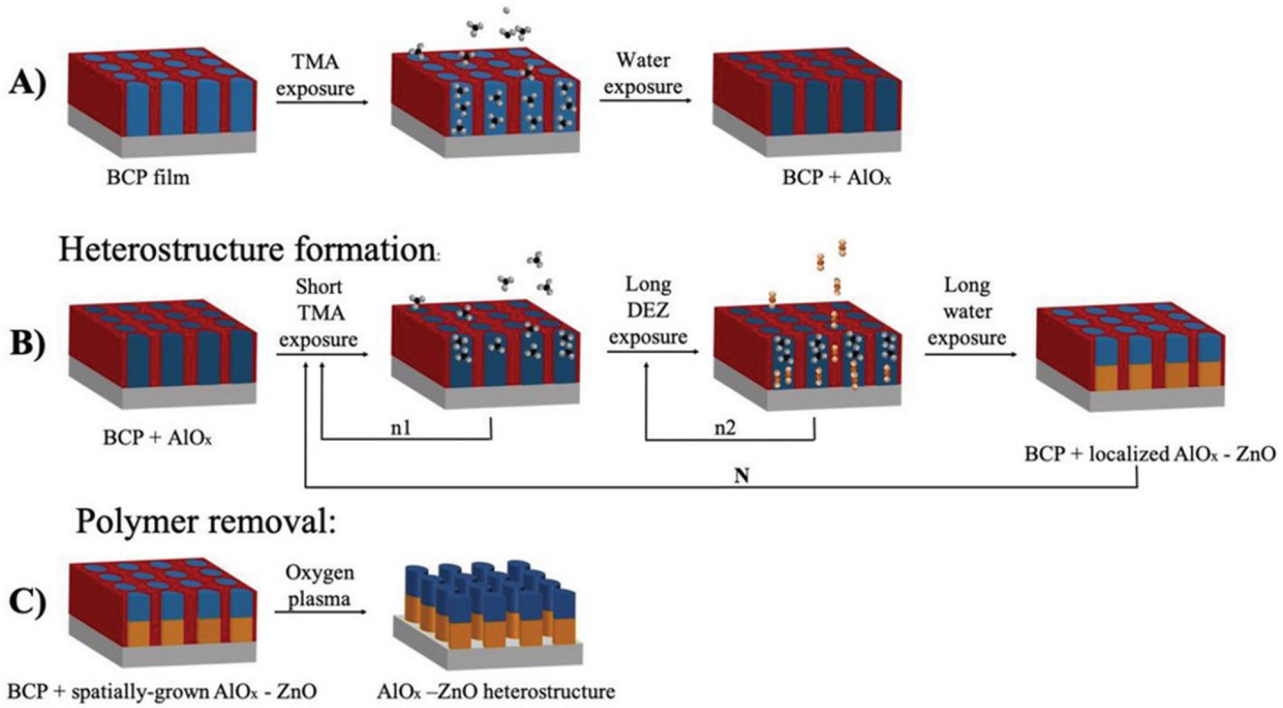

FIG. 12. Schematic representation of the ZnO/Al_2O_3 heterostructure fabrication. (a) Priming of the PS-*b*-PMMA film with trimethyl aluminum (TMA) to provide reactive sites for the growth of ZnO. (b) Formation of the heterostructure by exposure to TMA and diethyl zinc (DEZ) in one growth cycle. DEZ will diffuse deeper into the film resulting in cylinders of ZnO capped with Al_2O_3. (c) Removal of the polymer matrix by oxygen plasma treatment. Reprinted with permission from Azoulay *et al.*, Small **15**, 51 (2019). Copyright 2019 Wiley-VCH.[163]

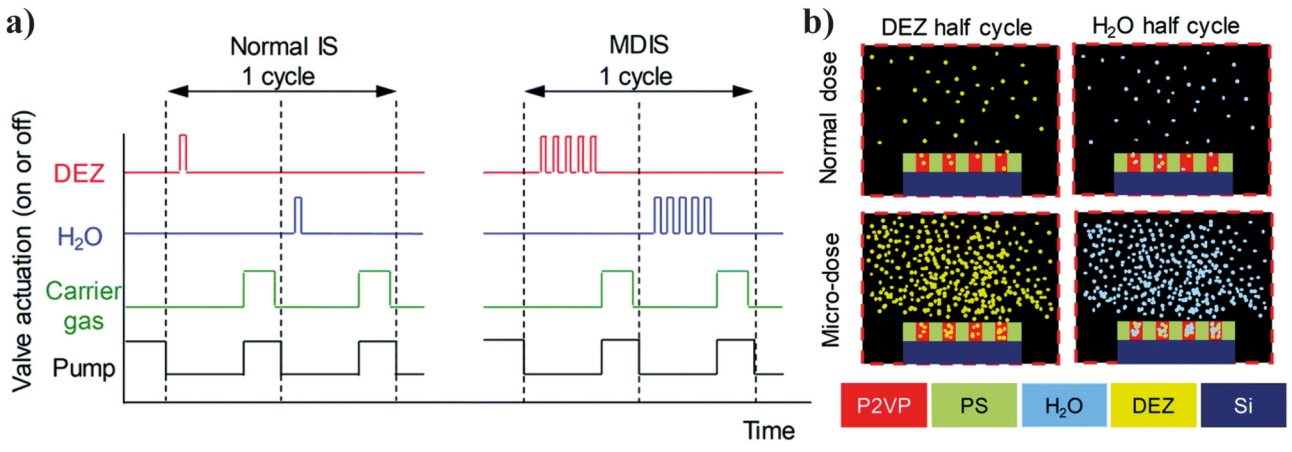

FIG. 13. (a) Schematic comparison between the pulse protocols normal infiltration synthesis (IS, left) and micro-dose infiltration synthesis (MDIS, right), showing an increased amount of precursor pulses [diethyl zinc (DEZ), H_2O] for the MDIS protocol. (b) Schematic representation of the difference in the precursor concentration in the reaction chamber for normal IS (top) and MDIS (bottom). Adapted with permission Subramanian *et al.*, Nanoscale **11**, 9533 (2019). Copyright 2019 The Royal Society of Chemistry, with permission conveyed through Copyright Clearance Center, Inc.

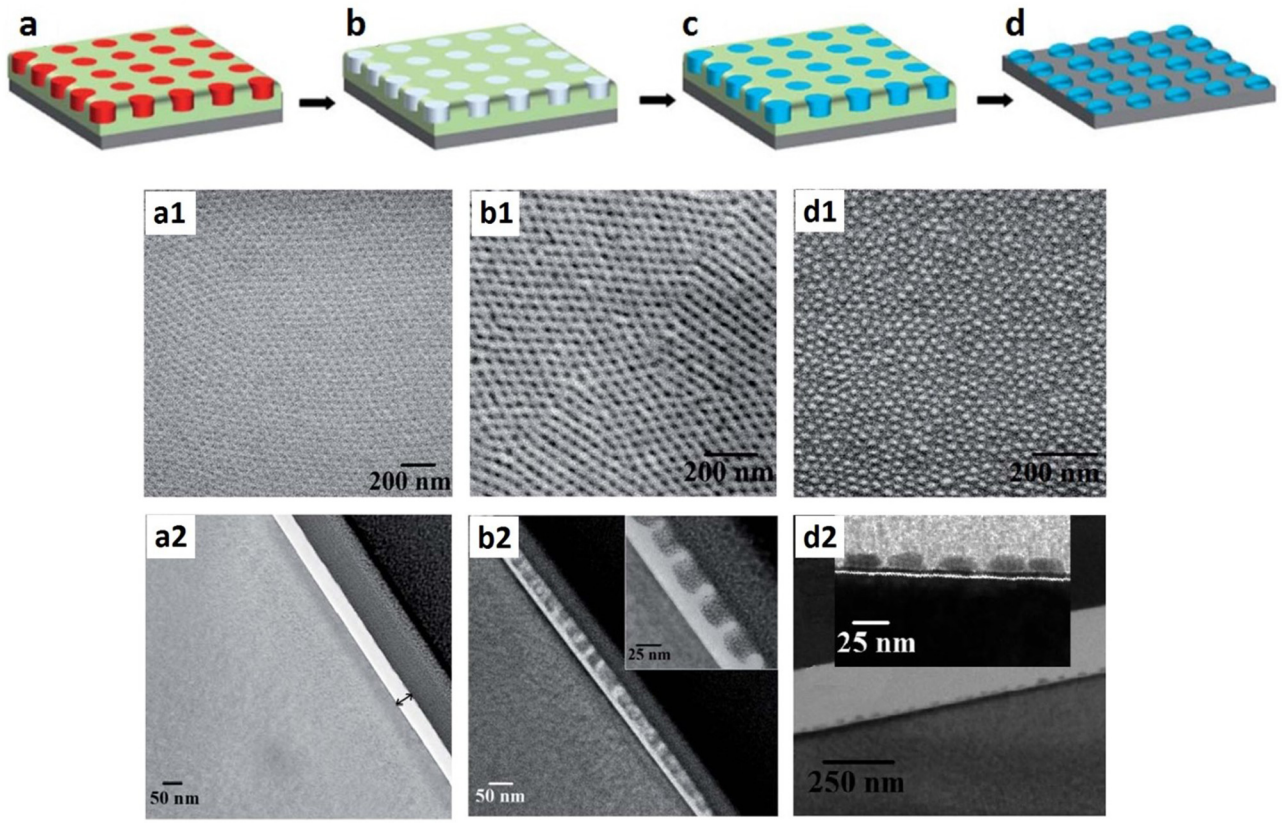

FIG. 14. [(a), (a1), and (a2)] SVA treated BCP thin film; [(b), (b1), and (b2)] BCP film after ethanol reconstruction; (c) BCP films with the PEO phase loaded with metal cations; [(d), (d1), and (d2)] oxide nanodots obtained after UV/O_3 and thermal treatment, where (a)–(d) are schematic illustration of the steps, [(a1), (b1), and (d1)] are top view SEM images, and [(a2), (b2), and (d2)] are cross-sectional TEM images. Adapted with permission of Ghoshal *et al.*, J. Mater. Chem. **22**, 12083 (2012). Copyright 2012 The Royal Society of Chemistry, permission conveyed through Copyright Clearance Center, Inc.

obtained after SVA in toluene + H_2O mixed vapor. Those films were later reconstructed [Figs. 14(b), 14(b1), and 14(b2)] via increased crystallization of the PEO block after soaking in ethanol for 15 h. PS is hydrophobic and insoluble in ethanol, while PEO is highly ethanol-soluble, metal cations were selectively loaded into the PEO phase during the spin coating of ethanol-based precursors [Fig. 14(c)]. Subsequent UV/O_3 treatment oxidized the cations and partially removed the template. Thermal annealing in the last step completely removed the organic residue and crystallized oxide nanodots [Figs. 14(d), 14(d1), and 14(d2)]. This approach is similar to the earlier work of the Shipp and co-workers[174] and Kim and co-workers,[175] in which polystyrene-block-poly(4-vinyl pyridine) (PS-*b*-P4VP) was used as a template. No surface reconstruction was required, instead, ions were loaded by immersing the films in the precursor solution. Oxygen plasma was performed to oxidize the nanodots instead of UV/O_3 plus thermal annealing. The loaded cations can also be oxidized by chemical reactions (e.g., with ammonia).[176,177]

Apart from cations, molecules or organometallic compounds containing the concerned elements can serve as precursors for oxides as well, for example, polydimethylsiloxane (PDMS) for silica[178] and ferrocene acetic acid [131] for iron oxide. A few special polymers contain blocks with the desired element. Those can be oxidized directly after SVA, without the need to load cations. For example, PS-*b*-PDMS thin films were transformed into silica nanowires,[179] and ferrocene triblock copolymers were transformed into iron oxide nanodots.[180]

Recently, Xu *et al.* reported the fabrication of nanodots of the complex oxide cobalt ferrite ($CoFe_2O_4$) by CSD, using acetylacetonate-based precursors of iron and cobalt with PS-*b*-PEO as the BCP template. The self-assembled BCP films were loaded with the precursor solution by immersion at elevated temperatures. Afterward, the films were treated with UV/O_3 and thermally annealed to oxidize the metal precursors and to remove the polymer matrix. This is one of the few reports of the fabrication of complex oxides using BCP templating.[142,152]

Horizontal morphologies (with no or limited long range order) such as lamella or horizontal cylinders are not often used for templating of metal oxides using CSD. Previously, metallic nanostructures have been formed using lamellar BCP and CSD to

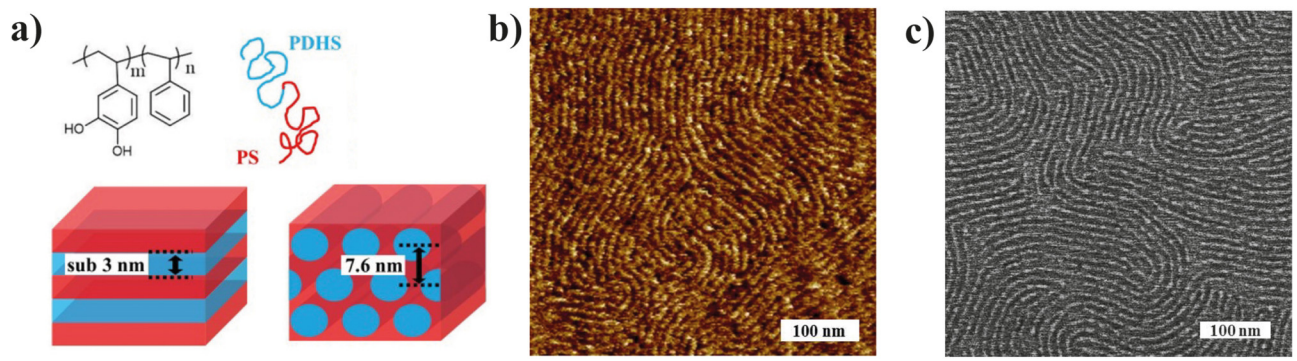

FIG. 15. (a) PDHS-b-PS and dimensions of the domains for the lamellar and cylindrical morphologies. (b) Tapping mode AFM image of the self-assembled fingerprint structure of the parallel cylindrical phase. (c) SEM image of the templated ZrO_2 structure after removal of the polymer matrix by O_2 plasma treatment. Adapted with permission Kwak *et al.*, Macromolecules **50**, 6813 (2017). Copyright 2017 American Chemical Society.

form metallic nanolines of metals such as Pt, Au, and Pd.[146,147,181–183] Only a few examples exist for the fabrication of simple oxides using CSD for horizontal morphologies,[184] sequential infiltration synthesis (Sec. III A) is more generally used in these cases for the fabrication of (simple) metal oxides.[149,158,159,161,163,166]

We predict that the best way to reduce the feature size of the BCP template features is to use high-χ polymers. These polymers have a high Flory–Huggins interaction parameter (χ) between the two blocks, which means the polymer blocks are more incompatible. High χ value BCPs have shown to produce small, sub-10 nm, domain spacings.[185–187] Such small feature sizes could be very interesting for lithography applications in the semiconductor and microelectronics industries. In 2015, Schulze *et al.*[186] reported the use of a high χ BCP to fabricate a hexagonally packed array of sub-10 nm metal oxide nanoparticles using a CSD method. They spin coated thin films of poly(cyclohexylethylene)-*block*-poly-(ethylene oxide) (PCEO-*b*-PEO, $\chi = 0.46$), which self-assembled into an array of nanodots with SVA treatment. The annealed films were loaded with alcohol-based metal precursor solutions by spin coating, with the precursors being selectively included in the PEO domains. UV/O_3 treatment oxidized the precursors and removed the polymer matrix, resulting in nanodot arrays of iron oxide, silicon oxide, and titanium oxide. This was the first study to show an etchless approach, using a selective inclusion method, for templating using high χ BCPs.

Challenging for high χ BCPs is the formation of perpendicular structures due to preferential interactions with non-neutral surfaces and segregation of one of the blocks to the free surface.[188] Yoshimura *et al.*[188] reported a fabrication method using a polymer brush to create a neutral surface. A 1.2 wt. % solution of polystyrene-*block*-poly[2-hydroxy-3-(2,2,2trifluoroethylsulfanyl)propyl methacrylate] (PS-*b*-PHFMA) ($\chi = 0.191$ at 25 °C) was spin coated and annealed at 120 °C for 10 min to create a perpendicular lamellar structure. These lamella showed a domain spacing of 9.6 nm, resulting in a sub-5 nm half-pitch. The PHFMA domain could be selectively removed using O_2-RIE, leaving a template that could be used for lithographic applications.

Sub-3 nm features were achieved by Kwak *et al.*[187] using polydihydroxystyrene-*block*-polystyrene (PDHS-*b*-PS, $\chi = 0.7$ at 170 °C) in the lamellar morphology (Fig. 15). The cylindrical morphology could be obtained by hanging the volume fraction of PS, resulting in cylinders with a 4 nm diameter and 8.8 nm center-to-center spacing. Thin films of the cylindrical phase were prepared, where the cylinders lay parallel to the substrate surface, sequential infiltration synthesis was used to incorporate a zirconium precursor into the PDHS block, followed by O_2 plasma etching to fabricate high density ZrO_2 nanowires.

C. Other polymer-based templating methods

In addition to BCPs, nanopatterned homopolymer or random copolymer thin films have been used to template oxide nanostructures during CSD as well. Dravid and co-workers[36,37,189–191] used the soft-EBL route described in Sec. II D, in which sols were spin-coated onto an EBL-patterned thin film of polymer resist. Low-temperature gelation followed by high-temperature pyrolysis converted sols into oxides and removed the polymer template simultaneously. A schematic illustration of the fabrication process is shown in Fig. 16(a). Various nanostructures of different types of oxides have been deposited using this method.[37,189–194] Figures 16(b)–16(d) illustrate a nanodisk structure of CFO as an example. Unlike BCP templating, soft-EBL is not limited by the very few possible nanostructures created by self-assembly, and size tuning does not require the synthesis of new BCPs. However, the soft-EBL approach is far less efficient and much more expensive than BCP templating.

Carretero-Genevrier *et al.*[195–198] used energetic and heavy ions to create nanopores in polycarbonate or polyimide films. The track-etched films were used as templates for solgel deposition. High aspect ratio free-standing nanopillars and nanowires of oxides such as quartz, $La_{0.7}Sr_{0.3}MnO_3$ (LSMO), $BaMn_8O_{16}$, and $SrMn_8O_{16}$ were fabricated. As an example, SEM images of track-etched polycarbonate films and as-obtained LSMO nanorods are shown in Fig. 17. The location and shape of the ion-etched pores cannot be properly controlled and, consequently, the oxide nanorods are randomly grown on the substrate and exhibit a large distribution on shape and size.

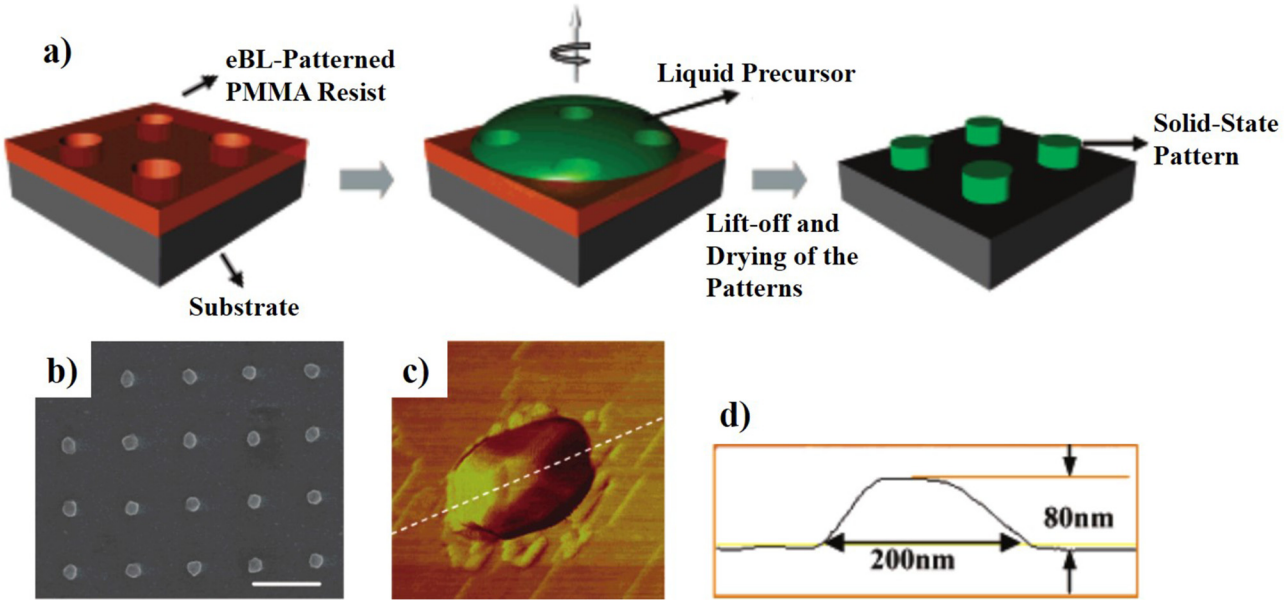

FIG. 16. (a) Schematic illustration of the soft-EBL patterning process, (b) SEM image of arrays of CFO nanodisks obtained from soft-EBL (scale bar 1 μm); (c) AFM image of one of the nanodisks; (d) profile along the white line in (c). Adapted with permission from Pan *et al.*, Nano Lett. **6**, 2344 (2006). Copyright 2006 American Chemical Society.

Polymer thin films patterned with surface relief grating (SRG) were also used to template oxide nanostructures. The Kim group[199,200] first combined SRGs and solgel deposition of oxides. They exposed azobenzene-functionalized polymer thin films with interferenced Ar + laser beams. Line trenches or square pitches were created in the exposed areas, due to a trans–cis transformation induced shrinkage. Pyrolysis after solgel deposition in the SRG-patterned films created oxide nano lines or nanoholes.

Finally, polymeric colloids are another type of template used in CSD of oxide nanostructures.[201,202] Li *et al.*[203] deposited silica nanomesh and ZnO nanopillars relying on the PS colloidal monolayer. A typical fabrication approach is schematically illustrated in Fig. 18.

Multiblock copolymers are also interesting for pattern transfer through templating or lithography. ABC triblock terpolymers give rise to more morphologies than accessible with diblock copolymers, which can lead to interesting new patterns (Fig. 19).[204–207] So far, these multiblock copolymer systems are mostly applied as etching masks or for lithographic pattern transfer. However, they pose an interesting direction with possibilities to be applied in polymer templating of metal oxides.

In 2006, Aizawa and Buriak[208] demonstrated the first use of an ABC triblock terpolymer [polystyrene-*block*-poly(2-vinylpyridine)-*block*-poly(ethylene oxide), PS-*b*-P2VP-*b*-PEO] to template two different metals at the same time. The polymer

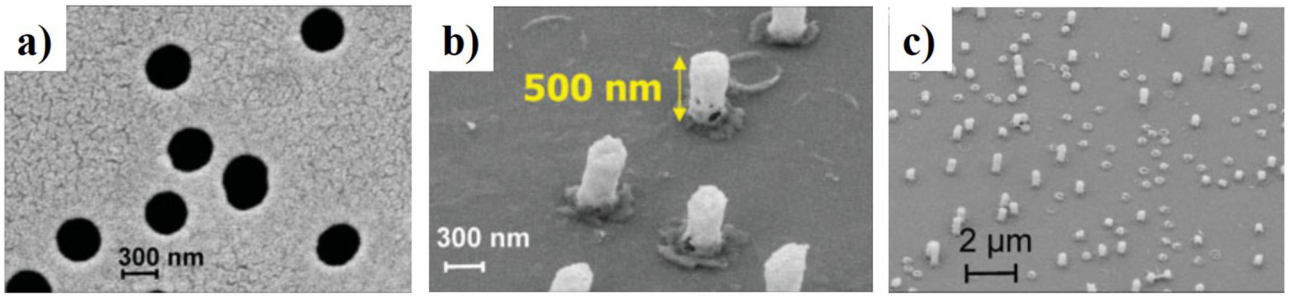

FIG. 17. SEM images of (a) track-etched polycarbonate film, (b) and (c) LSMO nanorods obtained from the polymer template. Adapted with permission from Carretero-Genevrier *et al.*, Adv. Funct. Mater. **20**, 892 (2010). Copyright 2010 Wiley-VCH.

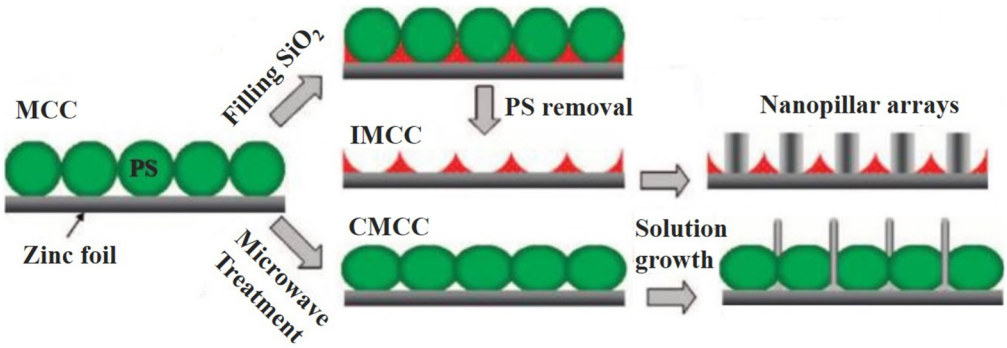

FIG. 18. Schematic illustration of the formation of ZnO nanopillars using a monolayer of colloidal crystals (MCC), an inverted MCC (IMCC), and a connected MCC (CMCC). Adapted with permission from Li *et al.*, Chem. Mater. **21**, 891 (2009). Copyright 2009 American Chemical Society.

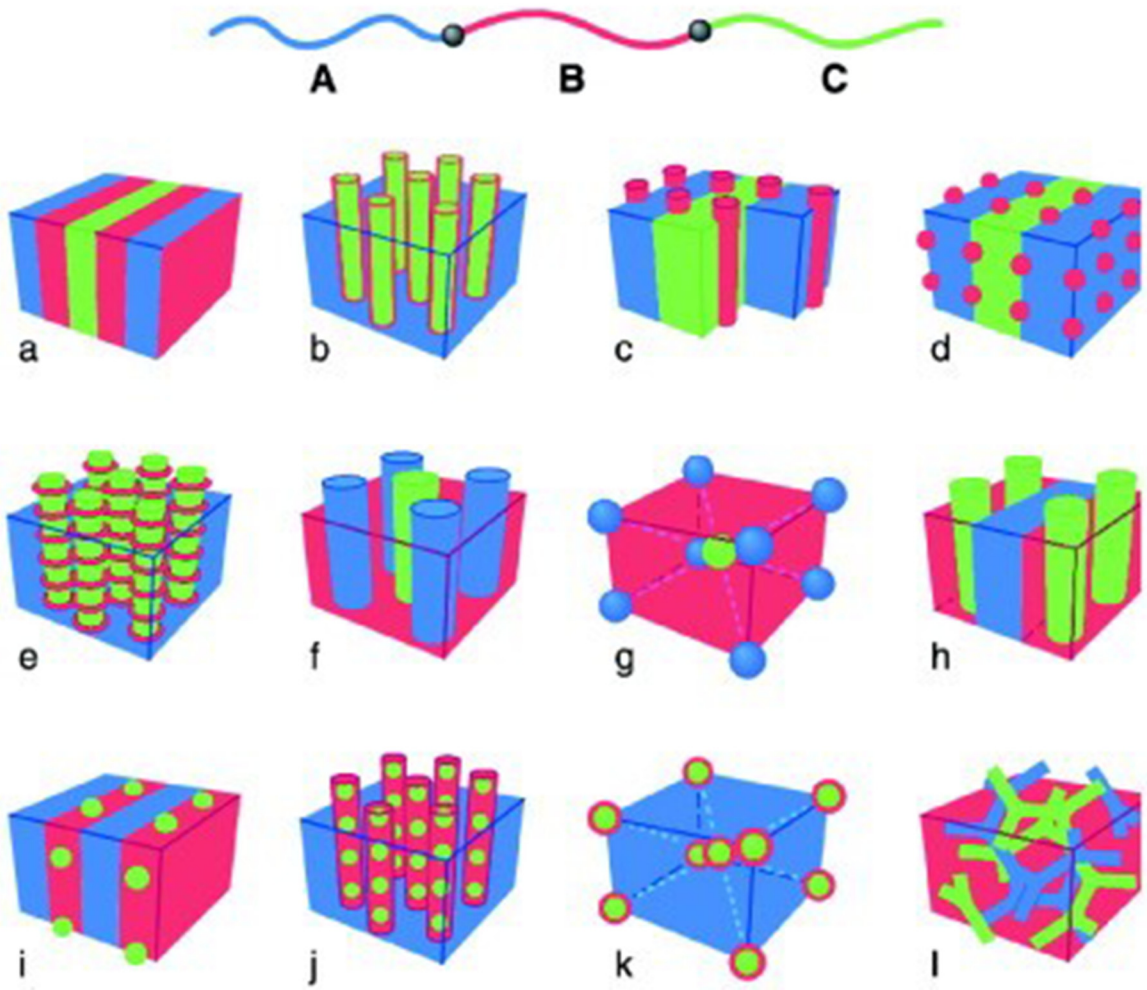

FIG. 19. Schematic representation of possible morphologies for a linear ABC triblock terpolymer. Adapted from Park *et al.*, Polymer **44**, 6725 (2003). Copyright 2003 Elsevier.

self-assembled in rod-shaped and spherical micelles with a PS core and a P2VP shell, surrounded by a PS matrix. One of the metal precursors (Au, Pt, or Pd) showed selectivity for the P2VP block, while the other metal precursor (Ag or Cu) would only penetrate the PEO block, allowing for the fabrication of sub-100 nm structures of Au (Pt or Pd) surrounded by Ag (Cu) films.

However, more common is the fabrication of etch masks or templates for lithographic pattern transfer using multiblock copolymers. Kubo *et al.*[209] reported that the ABC triblock terpolymer polystyrene-*block*-polyisoprene-*block*-polylactide (PS-*b*-PI-*b*-PLA) showed spontaneous alignment after spin coating, removing the need for additional annealing or alignment steps, due to the preference of PI to be at the surface and a non-preferential interaction between PS and PLA. These restrictions result in the formation of perpendicular hexagonally packed cylinders of a PLA core with a PI shell in the PS matrix. The PLA block can be removed by aqueous degradation, leaving a porous structure that could be used for pattern transfer.

A triblock copolymer, polylactide-*block*-poly(dimethylsiloxane)-*block*-polylactide (PLA-*b*-PDMS-*b*-PLA), was used by Rodwogin *et al.*,[210] and this block copolymer formed hexagonally packed perpendicular cylinders of PMMA in a PLA matrix. Through selective etching of the blocks, both dot and antidot arrays could be obtained; the PLA block could be etched by O_2 RIE, leaving an array of dots, whereas the PDMS block could be etched by fluorinated etchants, resulting in an antidot array. Using this method, they fabricated an array of gold nanodots, showing the possible application of this polymer system as a pattern transfer mask.

One of the interesting morphologies that are accessible through the use of ABC triblock terpolymers is the square symmetry cylindrical pattern, a symmetry that is of interest for the fabrication of integrated circuits. Son *et al.*[211] were the first to demonstrate a highly ordered square pattern using polyisoprene-*block*-polystyrene-*block*-polyferrocenylsilane (PI-*b*-PS-*b*-PFS), where PI and PFS form a square-symmetry arrangement in a PS matrix (Fig. 20). O_2 plasma etching was used to remove the PS and PI blocks, to leave the etch resistant PFS cylinders. These square arrays could be used as etch masks for other materials.

While the previously mentioned multiblock copolymer methods were mainly used for etch masks and lithographic pattern transfer, they could be of interest for templating using solution or vapor-based methods. Specifically, polymer blocks such as PI, P2VP, and PEO allow for selective incorporation of metal precursors, enabling the fabrication of metal oxide nanostructures.

It would be interesting to review the properties of the metal oxide nanostructures fabricated through polymer templating and compare the properties of each system grown by chemical deposition techniques vs physical vapor deposition (PVD) techniques. However, next to crystallinity, there is limited information available on other material properties for the systems that were discussed in Sec. III. Reports on BCP templated materials from Secs. III A and III B generally only include crystallinity, with one report of electrical properties as a function of the number of nanostructured layers in a 3D nanomesh[149] and one report of magnetic properties.[142] Publications on materials fabricated by non-BCP polymeric templating (Sec. III C) do report material properties more often; these

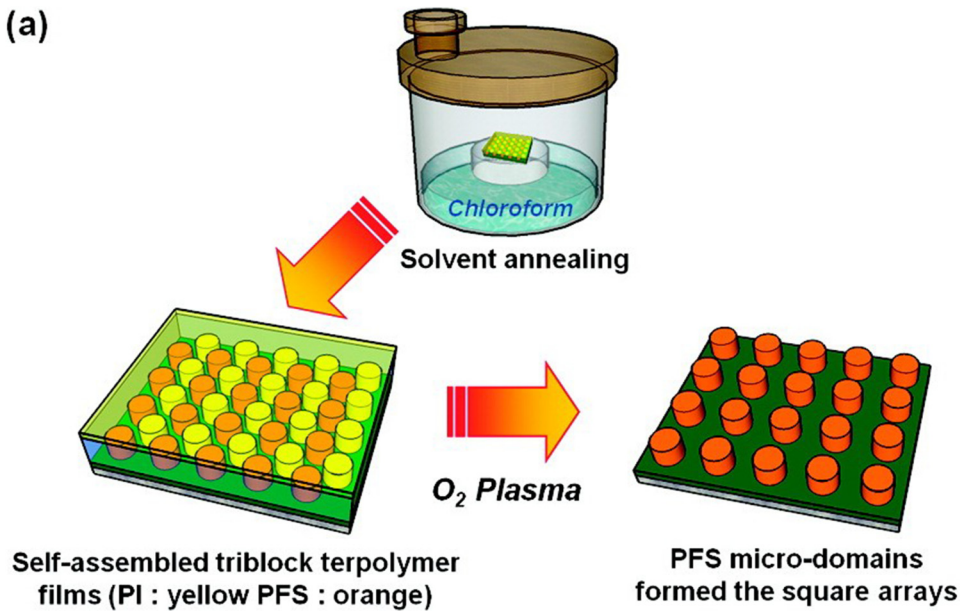

FIG. 20. Self-assembly of polyisoprene-*block*-polystyrene-*block*-polyferrocenylsilane (PI-*b*-PS-*b*-PFS) films forming a square array of PI (yellow) and PFS (orange) cylinders in a PS matrix. The PI and PS blocks are removed through O_2 plasma etching, resulting in a square array of PFS cylinders. Adapted with permission from Son *et al.*, Nano Lett. **11**, 2849 (2011). Copyright 2011 American Chemical Society.

reports generally discuss magnetic properties or piezoelectric coefficients, where the obtained values are generally comparable to literature values of either bulk or nanoscopic materials grown by different methods.[192,194–197] Therefore, we here focus the discussion on the crystalline properties. The crystalline properties of the fabricated metal oxide nanostructures mainly depend on the deposition method (CSD, ALD, PLD, etc.) and are less dependent on the method of templating. Typically, it is more challenging to obtain high-quality crystalline structures through CSD methods compared to ALD or PLD, especially considering epitaxial growth. For CSD methods, the obtained materials are generally not epitaxial, but high degrees of crystallinity can be obtained. Generally, grain growth within the polymer template results in polycrystalline nanostructures.[36,152,192] Single crystalline nanostructures can be obtained by CSD methods. However, the resulting nanostructures generally have a non-unified crystal orientation, resulting in an overall polycrystalline structure.[140,142,196,197] Epitaxial quality through CSD growth was so far only reported for metal oxides grown in non-BCP polymeric templates.[118,190,194] Limited by the phase transition temperature or decomposition temperature of the polymer templates, relatively low deposition temperatures are typically used during polymer-templated ALD. Therefore, achieving epitaxial quality using polymer-templated ALD deposition is also challenging. The materials discussed in this review that were grown through SIS are also polycrystalline.

IV. SUMMARY AND OUTLOOK

The nano-structuring of complex oxide composites to form regular patterns with a variety of morphologies is of great interest to achieve large area multifunctional thin layers. These composite materials offer the combined functionality of their components but also an increase in the interface area between them in order to optimize the coupling between their individual properties, as in the case of the magneto-electric coupling of composites made of piezoelectric and magnetostrictive components. In the past few decades, several methods have been put forward to achieve such materials.

In this Perspective, we have put the recent progress in this direction into context with an emphasis on polymer templating-based solutions as low-cost methods to achieve large areas of nanostructured oxide composites. The recent results in this context clearly show the superiority of this relatively easy approach. We can predict that this technique will lead to disruptive technologies when other BCPs—in terms of chemistry, composition, dispersities etc.—will be used in the near future. This can already be seen in the few recent examples using multi-block copolymers.

One of the most promising directions for future research is the use of high χ BCPs since they allow for sub-10 nm feature sizes, with the smallest features reported to date at sub-3 nm.[185–187] Developing this technology further calls for an intensified collaboration between synthetic polymer chemists that develop novel BCPs with even increased χ parameter difference and tailored morphologies and applied device physicists to drive this field.

Additionally, interesting new and complex morphologies can be obtained through the combination of different BCP morphologies and by layering to create 3D nanostructures.[166,212–214] Directed self-assembly approaches will be used to further tailor and miniaturize the desired structures. In combination with high χ BCPs, these will be powerful patterning techniques that will outperform traditional PLD technologies by ease, design flexibility, and performance.

Another direction in which we can foresee increasing interest is the fabrication of complex oxide nanostructures through BCP templating, so far mostly simple oxides have been fabricated in this way, but complex oxides offer a large spectrum of ordering phenomena (ferroelectricity, ferromagnetism, ferroelasticity, orbital ordering, metal–insulator transformations, etc.) that allow different physical properties to be tuned in a very controlled manner by using electric fields, magnetic fields, light, strain, or confinement, which makes them highly fitting for applications in memory storage, logic, sensing, or adaptable electronics.

Further development of these approaches will make BCP templating suitable for the fabrication of devices for the semiconductor or microelectronics industry, while using low temperature, low cost fabrication methods. We hope that this Perspective will encourage scientists in the oxide community to make use of these highly promising tools and will help to increase the synergy between these two communities.

AUTHORS' CONTRIBUTIONS

J.X. and A.I.B. contributed equally to this work.

ACKNOWLEDGMENTS

This research was financially supported by grants from the Zernike Institute for Advanced Materials (ZIAM), the Netherlands Organization for Scientific Research (NWO), and the Ubbo Emmius Funds of the University of Groningen.

DATA AVAILABILITY

Data sharing is not applicable to this article as no new data were created or analyzed in this study.

REFERENCES

[1]U. C. Chung, C. Elissalde, S. Mornet, M. Maglione, and C. Estournès, Appl. Phys. Lett. **94**, 072903 (2009).
[2]A. S. Everhardt, T. Denneulin, A. Grünebohm, Y.-T. Shao, P. Ondrejkovic, S. Zhou, N. Domingo, G. Catalan, J. Hlinka, J.-M. Zuo, S. Matzen, and B. Noheda, Appl. Phys. Rev. **7**, 011402 (2020).
[3]T. Liu, H. Zhang, F. Wang, J. Shi, P. Ci, L. Wang, S. Ge, Q. Wang, and P. K. Chu, Mater. Sci. Eng., B **176**, 387 (2011).
[4]Z. L. Wang, J. Phys. Condens. Matter **16**, R829 (2004).
[5]X. Wang, C. J. Summers, and Z. L. Wang, Nano Lett. **4**, 423 (2004).
[6]X. Wang, J. Zhou, J. Song, J. Liu, N. Xu, and Z. L. Wang, Nano Lett. **6**, 2768 (2006).
[7]V. Suresh, M. S. Huang, M. P. Srinivasan, C. Guan, H. J. Fan, and S. Krishnamoorthy, J. Phys. Chem. C **116**, 23729 (2012).
[8]L. Gao, P.-Y. Chen, and S. Yu, Appl. Phys. Lett. **111**, 103503 (2017).
[9]S. Kumar, J. P. Strachan, and R. S. Williams, Nature **548**, 318 (2017).
[10]S. Kumar and R. S. Williams, Nat. Commun. **9**, 2030 (2018).
[11]D. Lee, E. Cha, J. Park, C. Sung, K. Moon, S. A. Chekol, and H. Hwang, IEEE J. Electron Devices Soc. **1**, 250 (2018).
[12]D. Lee, M. Kwak, K. Moon, W. Choi, J. Park, J. Yoo, J. Song, S. Lim, C. Sung, W. Banerjee, and H. Hwang, Adv. Electron. Mater. **5**, 1800866 (2019).

[13]A. C. Kozen, Z. R. Robinson, E. R. Glaser, M. Twigg, T. J. Larrabee, H. Cho, S. M. Prokes, and L. B. Ruppalt, ACS Appl. Mater. Interfaces **12**, 16639 (2020).
[14]W. Yi, K. K. Tsang, S. K. Lam, X. Bai, J. A. Crowell, and E. A. Flores, Nat. Commun. **9**, 4661 (2018).
[15]Z. You and S. Ramanathan, Proc. IEEE **103**, 1289 (2015).
[16]B. Zhao and J. Ravichandran, Phys. Rev. Appl. **11**, 014020 (2019).
[17]J. Lappalainen, J. Mizsei, and M. Huotari, J. Appl. Phys. **125**, 044501 (2019).
[18]R. E. Newnham and S. Trolier-McKinstry, J. Appl. Crystallogr. **23**, 447 (1990).
[19]J. F. Scott, Nat. Mater. **6**, 256 (2007).
[20]Z. Shi, C. Wang, X. Liu, and C. Nan, Sci. Bull. **53**, 2135 (2008).
[21]J. Ruan, X. Qiu, Z. Yuan, D. Ji, P. Wang, A. Li, and D. Wu, Appl. Phys. Lett. **107**, 232902 (2015).
[22]D. H. A. Blank, M. Dekkers, and G. Rijnders, J. Phys. D Appl. Phys. **47**, 034006 (2014).
[23]S. H. Lee, G. Tian, T. C. Kim, H. K. Jung, J. W. Choi, F. J. Walker, C. H. Ahn, C. A. Ross, and D. H. Kim, Nanotechnology **30**, 105601 (2019).
[24]T. C. Kim, S. Ojha, G. Tian, S. H. Lee, H. K. Jung, J. W. Choi, L. Kornblum, F. J. Walker, C. H. Ahn, C. A. Ross, and D. H. Kim, J. Mater. Chem. C **6**, 5552 (2018). 3
[25]D. G. Schlom, L.-Q. Chen, C.-B. Eom, K. M. Rabe, S. K. Streiffer, and J.-M. Triscone, Annu. Rev. Mater. Res. **37**, 589 (2007).
[26]L. W. Martin, Y. H. Chu, and R. Ramesh, Mater. Sci. Eng., R **68**, 89 (2010).
[27]R. Scherwitzl, P. Zubko, C. Lichtensteiger, and J. M. Triscone, Appl. Phys. Lett. **95**, 222114 (2009).
[28]M. Ritala, Science **288**, 319 (2000).
[29]M. Leskelä and M. Ritala, Thin Solid Films **409**, 138 (2002).
[30]M. D. Groner, J. W. Elam, F. H. Fabreguette, and S. M. George, Thin Solid Films **413**, 186 (2002).
[31]D. M. Hausmann, E. Kim, J. Becker, and R. G. Gordon, Chem. Mater. **14**, 4350 (2002).
[32]R. W. Johnson, A. Hultqvist, and S. F. Bent, Mater. Today **17**, 236 (2014).
[33]M. Coll and M. Napari, APL Mater. **7**, 110901 (2019).
[34]L. Francioso, A. Taurino, A. Forleo, and P. Siciliano, Sens. Actuators B **130**, 70 (2008).
[35]F. Stehlin, F. Wieder, A. Spangenberg, J.-M. Le Meins, and O. Soppera, J. Mater. Chem. C **2**, 277 (2014).
[36]Z. Pan, S. K. Donthu, N. Wu, S. Li, and V. P. Dravid, Small **2**, 274 (2006).
[37]Z. Pan, S. Li, Z. Wang, M.-F. Yu, and V. P. Dravid, Appl. Phys. Lett. **91**, 143105 (2007).
[38]R. Comes, H. Liu, M. Khokhlov, R. Kasica, J. Lu, and S. A. Wolf, Nano Lett. **12**, 2367 (2012).
[39]S. M. Stratulat, X. Lu, A. Morelli, D. Hesse, W. Erfurth, and M. Alexe, Nano Lett. **13**, 3884 (2013).
[40]X. L. Lu, J. W. Zhang, C. F. Zhang, J. C. Zhang, and Y. Hao, RSC Adv. **5**, 58640 (2015).
[41]Y. Wang, J. Hu, Y. Lin, and C.-W. Nan, NPG Asia Mater. **2**, 61 (2010).
[42]C.-W. Nan, M. I. Bichurin, S. Dong, D. Viehland, and G. Srinivasan, J. Appl. Phys. **103**, 031101 (2008).
[43]J. Van Den Boomgaard, D. R. Terrell, R. A. J. Born, and H. F. J. I. Giller, J. Mater. Sci. **9**, 1705 (1974).
[44]A. M. J. G. Van Run, D. R. Terrell, and J. H. Scholing, J. Mater. Sci. **9**, 1710 (1974).
[45]J. Ryu, A. V. Carazo, K. Uchino, and H.-E. Kim, J. Electroceram. **7**, 17 (2001).
[46]K. K. Patankar, R. P. Nipankar, V. L. Mathe, R. P. Mahajan, and S. A. Patil, Ceram. Int. **27**, 853 (2001).
[47]J. Zhai, N. Cai, Z. Shi, Y. Lin, and C.-W. Nan, J. Appl. Phys. **95**, 5685 (2004).
[48]G. Srinivasan, C. P. DeVreugd, C. S. Flattery, V. M. Laletsin, and N. Paddubnaya, Appl. Phys. Lett. **85**, 2550 (2004).
[49]Q. H. Jiang, Z. J. Shen, J. P. Zhou, Z. Shi, and C.-W. Nan, J. Eur. Ceram. Soc. **27**, 279 (2007).
[50]J. Ryu, C.-W. Baek, G. Han, C.-S. Park, J.-W. Kim, B.-D. Hahn, W.-H. Yoon, D.-S. Park, S. Priya, and D.-Y. Jeong, Ceram. Int. **38**, S431 (2012).
[51]J.-G. Wan, H. Zhang, X. Wang, D. Pan, J.-M. Liu, and G. Wang, Appl. Phys. Lett. **89**, 122914 (2006).
[52]S. Q. Ren, L. Q. Weng, S. H. Song, F. Li, J. G. Wan, and M. Zeng, J. Mater. Sci. **40**, 4375 (2005).
[53]P. Martins, X. Moya, C. Caparrós, J. Fernandez, N. D. Mathur, and S. Lanceros-Mendez, J. Nanopart. Res. **15**, 1825 (2013).
[54]D. Bhadra, M. G. Masud, S. K. De, and B. K. Chaudhuri, Appl. Phys. Lett. **102**, 072902 (2013).
[55]A. Mayeen, S. K. M, S. J. M, S. Thomas, J. Philip, D. Rouxel, R. N. Bhowmik, and N. Kalarikkal, Dalton Trans **48**, 16961 (2019).
[56]M. M. Fernandes, H. Mora, E. D. Barriga-Castro, C. Luna, R. Mendoza-Reséndez, C. Ribeiro, S. Lanceros-Mendez, and P. Martins, J. Phy. Chem. C **122**, 19189 (2018).
[57]R. A. Islam, Y. Ni, A. G. Khachaturyan, and S. Priya, J. Appl. Phys. **104**, 044103 (2008).
[58]G. Srinivasan, E. T. Rasmussen, J. Gallegos, R. Srinivasan, Y. I. Bokhan, and V. M. Laletin, Phys. Rev. B **64**, 214408 (2001).
[59]G. Srinivasan, E. T. Rasmussen, B. J. Levin, and R. Hayes, Phys. Rev. B **65**, 134402 (2002).
[60]Y. Wang, D. Gray, D. Berry, J. Gao, M. Li, J. Li, and D. Viehland, Adv. Mater. **23**, 4111 (2011).
[61]M. Silva, S. Reis, C. S. Lehmann, P. Martins, S. Lanceros-Mendez, A. Lasheras, J. Gutiérrez, and J. M. Barandiarán, ACS Appl. Mater. Interfaces **5**, 10912 (2013).
[62]Z. Shi, C. W. Nan, J. Zhang, N. Cai, and J.-F. Li, Appl. Phys. Lett. **87**, 012503 (2005).
[63]B. Y. Wang, H. T. Wang, S. B. Singh, Y. C. Shao, Y. F. Wang, C. H. Chuang, P. H. Yeh, J. W. Chiou, C. W. Pao, H. M. Tsai, H. J. Lin, J. F. Lee, C. Y. Tsai, W. F. Hsieh, M. H. Tsai, and W. F. Pong, RSC Adv. **3**, 7884 (2013).
[64]A. McDannald, M. Staruch, G. Sreenivasulu, C. Cantoni, G. Srinivasan, and M. Jain, Appl. Phys. Lett. **102**, 122905 (2013).
[65]M. Liu, X. Li, J. Lou, S. Zheng, K. Du, and N. X. Sun, J. Appl. Phys. **102**, 083911 (2007).
[66]X. L. Zhong, J. B. Wang, M. Liao, G. J. Huang, S. H. Xie, Y. C. Zhou, Y. Qiao, and J. P. He, Appl. Phys. Lett. **90**, 152903 (2007).
[67]J. G. Wan, X. W. Wang, Y. J. Wu, M. Zeng, Y. Wang, H. Jiang, W. Q. Zhou, G. H. Wang, and J.-M. Liu, Appl. Phys. Lett. **86**, 122501 (2005).
[68]N. Ortega, P. Bhattacharya, R. S. Katiyar, P. Dutta, A. Manivannan, M. S. Seehra, I. Takeuchi, and S. B. Majumder, J. Appl. Phys. **100**, 126105 (2006).
[69]A. McDannald, L. Ye, C. Cantoni, S. Gollapudi, G. Srinivasan, B. D. Huey, and M. Jain, Nanoscale **9**, 3246 (2017).
[70]H. Ryu, P. Murugavel, J. H. Lee, S. C. Chae, T. W. Noh, Y. S. Oh, H. J. Kim, K. H. Kim, J. H. Jang, M. Kim, C. Bae, and J. G. Park, Appl. Phys. Lett. **89**, 102907 (2006).
[71]Y. G. Ma, W. N. Cheng, M. Ning, and C. K. Ong, Appl. Phys. Lett. **90**, 152911 (2007).
[72]C. Deng, Y. Zhang, J. Ma, Y. Lin, and C.-W. Nan, Acta Mater. **56**, 405 (2008).
[73]M. Ziese, A. Bollero, I. Panagiotopoulos, and N. Moutis, Appl. Phys. Lett. **88**, 212502 (2006).
[74]J. Chen, Z. Tang, and S. Zhao, J. Alloys Compd. **712**, 256 (2017).
[75]Y. Zhang, C. Deng, J. Ma, Y. Lin, and C.-W. Nan, Appl. Phys. Lett. **92**, 062911 (2008).
[76]H. C. He, J. Ma, Y. H. Lin, and C. W. Nan, J. Phys. D Appl. Phys. **42**, 095008 (2009).
[77]Z. Zheng, P. Zhou, Y. Liu, K. Liang, R. G. Tanguturi, H. Chen, G. Srinivasan, Y. Qi, and T. Zhang, J. Alloys Compd. **818**, 152871 (2020).
[78]H. C. He, J. Wang, J. P. Zhou, and C. W. Nan, Adv. Funct. Mater. **17**, 1333 (2007).
[79]S. Ryu, J. H. Park, and H. M. Jang, Appl. Phys. Lett. **91**, 142910 (2007).
[80]T. Li, D. Ma, K. Li, and Z. Hu, J. Alloys Compd. **747**, 558 (2018).
[81]J. A. Mundy, C. M. Brooks, M. E. Holtz, J. A. Moyer, H. Das, A. F. Rébola, J. T. Heron, J. D. Clarkson, S. M. Disseler, Z. Liu, A. Farhan, R. Held, R. Hovden, E. Padgett, Q. Mao, H. Paik, R. Misra, L. F. Kourkoutis, E. Arenholz, A. Scholl, J. A. Borchers, W. D. Ratcliff, R. Ramesh, C. J. Fennie, P. Schiffer, D. A. Muller, and D. G. Schlom, Nature **537**, 523 (2016).

[82]M. Liu, B. M. Howe, L. Grazulis, K. Mahalingam, T. Nan, N. X. Sun, and G. J. Brown, Adv. Mater. **25**, 4886 (2013).
[83]S. W. Yang, R. C. Peng, T. Jiang, Y. K. Liu, L. Feng, J. J. Wang, L. Q. Chen, X. G. Li, and C. W. Nan, Adv. Mater. **26**, 7091 (2014).
[84]M. Ghidini, F. Maccherozzi, X. Moya, L. C. Phillips, W. Yan, J. Soussi, N. Metallier, M. E. Vickers, N. J. Steinke, R. Mansell, C. H. Barnes, S. S. Dhesi, and N. D. Mathur, Adv. Mater. **27**, 1460 (2015).
[85]W. Eerenstein, M. Wiora, J. L. Prieto, J. F. Scott, and N. D. Mathur, Nat. Mater. **6**, 348 (2007).
[86]C. Thiele, K. Dörr, O. Bilani, J. Rödel, and L. Schultz, Phys. Rev. B **75**, 054408 (2007).
[87]T. Wu, M. A. Zurbuchen, S. Saha, R. V. Wang, S. K. Streiffer, and J. F. Mitchell, Phys. Rev. B **73**, 134416 (2006).
[88]J. Wang, Y. Zhang, J. Ma, Y. Lin, and C. W. Nan, J. Appl. Phys. **104**, 014101 (2008).
[89]X. Lu, S. Dong, X. Li, M. Alexe, D. Hesse, and Y. Hao, Appl. Phys. Lett. **101**, 222902 (2012).
[90]I. Fina, N. Dix, J. M. Rebled, P. Gemeiner, X. Marti, F. Peiro, B. Dkhil, F. Sanchez, L. Fabrega, and J. Fontcuberta, Nanoscale **5**, 8037 (2013).
[91]S. S. Nair, G. Pookat, V. Saravanan, and M. R. Anantharaman, J. Appl. Phys. **114**, 064309 (2013).
[92]C.-W. Nan, G. Liu, Y. Lin, and H. Chen, Phys. Rev. Lett. **94**, 197203 (2005).
[93]H. Zheng, J. Wang, S. E. Lofland, Z. Ma, L. Mohaddes-Ardabili, T. Zhao, L. Salamanca-Riba, S. R. Shinde, S. B. Ogale, F. Bai, D. Viehland, Y. Jia, D. G. Schlom, M. Wuttig, A. Roytburd, and R. Ramesh, Science **303**, 661 (2004).
[94]C. Schmitz-Antoniak, D. Schmitz, P. Borisov, F. M. de Groot, S. Stienen, A. Warland, B. Krumme, R. Feyerherm, E. Dudzik, W. Kleemann, and H. Wende, Nat. Commun. **4**, 2051 (2013).
[95]M. Rafique, A. Herklotz, E. J. Guo, R. Roth, L. Schultz, K. Dörr, and S. Manzoor, J. Appl. Phys. **114**, 233910 (2013).
[96]D. H. Kim, N. M. Aimon, X. Sun, and C. A. Ross, Adv. Funct. Mater. **24**, 2334 (2014).
[97]H. Zheng, Q. Zhan, F. Zavaliche, M. Sherburne, F. Straub, M. P. Cruz, L.-Q. Chen, U. Dahmen, and R. Ramesh, Nano Lett. **6**, 1401 (2006).
[98]F. Zavaliche, H. Zheng, L. Mohaddes-Ardabili, S. Y. Yang, Q. Zhan, P. Shafer, E. Reilly, R. Chopdekar, Y. Jia, P. Wright, D. G. Schlom, Y. Suzuki, and R. Ramesh, Nano Lett. **5**, 1793 (2005).
[99]Z. Wang, Y. Li, R. Viswan, B. Hu, V. G. Harris, J. Li, and D. Viehland, ACS Nano **7**, 3447 (2013).
[100]Z. Wang, Y. Zhang, Y. Wang, Y. Li, H. Luo, J. Li, and D. Viehland, ACS Nano **8**, 7793 (2014).
[101]G. Tian, S. Ojha, S. Ning, X. Gao, and C. A. Ross, Adv. Electron. Mater. **5**, 1900012 (2019).
[102]I. Levin, J. Li, J. Slutsker, and A. L. Roytburd, Adv. Mater. **18**, 2044 (2006).
[103]Z. Tan, A. L. Roytburd, I. Levin, K. Seal, B. J. Rodriguez, S. Jesse, S. Kalinin, and A. Baddorf, Appl. Phys. Lett. **93**, 074101 (2008).
[104]C. Y. Tsai, H. R. Chen, F. C. Chang, W. C. Tsai, H. M. Cheng, Y. H. Chu, C. H. Lai, and W. F. Hsieh, Appl. Phys. Lett. **102**, 132905 (2013).
[105]J.-G. Wan, Y. Weng, Y. Wu, Z. Li, J.-M. Liu, and G. Wang, Nanotechnology **18**, 465708 (2007).
[106]L.-Y. Ding, F.-X. Wu, Y.-B. Chen, Z.-B. Gu, and S.-T. Zhang, Appl. Surf. Sci. **257**, 3840 (2011).
[107]S. Ojha, W. C. Nunes, N. M. Aimon, and C. A. Ross, ACS Nano **10**, 7657 (2016).
[108]D. H. Kim, N. M. Aimon, and C. A. Ross, J. Appl. Phys. **113**, 17B510 (2013).
[109]D. H. Kim, T. C. Kim, S. H. Lee, S. H. Han, K.-S. Han, and C. A. Ross, J. Appl. Phys. **121**, 163902 (2017).
[110]X. C. Akira Imai, H. L. Xin, E. A. Eliseev, A. N. Morozovska, S. V. Kalinin, M. L. Ryota Takahashi, Y. Matsumoto, and V. Nagarajan, ACS Nano **7**, 11079 (2013).
[111]H. Zheng, F. Straub, Q. Zhan, P. L. Yang, W. K. Hsieh, F. Zavaliche, Y. H. Chu, U. Dahmen, and R. Ramesh, Adv. Mater. **18**, 2747 (2006).
[112]D. H. Kim, X. Sun, T. C. Kim, Y. J. Eun, T. Lee, S. G. Jeong, and C. A. Ross, ACS Appl. Mater. Interfaces **8**, 2673 (2016).
[113]N. M. Aimon, H. K. Choi, X. Y. Sun, D. H. Kim, and C. A. Ross, Adv. Mater. **26**, 3063 (2014).
[114]N. M. Aimon, D. H. Kim, X. Sun, and C. A. Ross, ACS Appl. Mater. Interfaces **7**, 2263 (2015).
[115]H. K. Choi, N. M. Aimon, D. H. Kim, X. Y. Sun, J. Gwyther, I. Manners, and C. A. Ross, ACS Nano **8**, 9248 (2014).
[116]D. H. Kim, S. Ning, and C. A. Ross, J. Mater. Chem. C **7**, 9128 (2019).
[117]H. Luo, H. Yang, S. A. Baily, O. Ugurlu, M. Jain, M. E. Hawley, T. M. McCleskey, A. K. Burrell, E. Bauer, L. Civale, T. G. Holesinger, and Q. Jia, J. Am. Chem. Soc. **129**, 14132 (2007).
[118]B. Liu, T. Sun, J. He, and V. P. Dravid, ACS Nano **4**, 6836 (2010).
[119]S. Ren, R. M. Briber, and M. Wuttig, Appl. Phys. Lett. **93**, 173507 (2008).
[120]H. K. Kim, L. T. Schelhas, S. Keller, J. L. Hockel, S. H. Tolbert, and G. P. Carman, Nano Lett. **13**, 884 (2013).
[121]H. Sohn, M. E. Nowakowski, C.-Y. Liang, J. L. Hockel, K. Wetzlar, S. Keller, B. M. McLellan, M. A. Marcus, A. Doran, A. Young, M. Kläui, G. P. Carman, J. Bokor, and R. N. Candler, ACS Nano **9**, 4814 (2015).
[122]X. Lu, Y. Kim, S. Goetze, X. Li, S. Dong, P. Werner, M. Alexe, and D. Hesse, Nano Lett. **11**, 3202 (2011).
[123]G. Tian, F. Zhang, J. Yao, H. Fan, P. Li, Z. Li, X. Song, X. Zhang, M. Qin, M. Zeng, Z. Zhang, J. Yao, X. Gao, and J. Liu, ACS Nano **10**, 1025 (2016).
[124]X. Gao, B. J. Rodriguez, L. Liu, B. Birajdar, D. Pantel, M. Ziese, M. Alexe, and D. Hesse, ACS Nano **4**, 1099 (2010).
[125]I. Vrejoiu, A. Morelli, D. Biggemann, and E. Pippel, Nano Rev. **2**, 7364 (2011).
[126]X. Wang, X. Wang, W. Huang, P. J. Sebastian, and S. Gamboa, J. Power Sources **140**, 211 (2005).
[127]S. Yue, Z. Yan, Y. Shi, and G. Ran, Mater. Lett. **98**, 246 (2013).
[128]O. D. Velev and A. M. Lenhoff, Curr. Opin. Colloid Interface Sci. **5**, 56 (2000).
[129]O. D. Velev and E. W. Kaler, Adv. Mater. **12**, 531 (2000).
[130]M. Kuemmel, J. Allouche, L. Nicole, C. Boissière, C. Laberty, H. Amenitsch, C. Sanchez, and D. Grosso, Chem. Mater. **19**, 3717 (2007).
[131]B. K. Kuila, M. S. Rama, and M. Stamm, Adv. Mater. **23**, 1797 (2011).
[132]M. Faustini, G. L. Drisko, A. A. Letailleur, R. S. Montiel, C. Boissière, A. Cattoni, A. M. Haghiri-Gosnet, G. Lerondel, and D. Grosso, Nanoscale **5**, 984 (2013).
[133]Q. Xu, J.-H. Smått, J. Peltonen, and P. Ihalainen, J. Mater. Res. **30**, 2151 (2015).
[134]A. Castro, P. Ferreira, and P. M. Vilarinho, J. Phys. Chem. C **120**, 10961 (2016).
[135]T. Bottein, M. Bouabdellaoui, J.-B. Claude, L. Favre, T. David, M. Putero, A. Ronda, M. Abbarchi, I. Berbezier, and D. Grosso, ACS Appl. Nano Mater. **2**, 2026 (2019).
[136]M. W. Matsen and F. S. Bates, Macromolecules **29**, 1091 (1996).
[137]I. W. Hamley, Nanotechnology **14**, R39 (2003).
[138]I. W. Hamley, Prog. Polym. Sci. **34**, 1161 (2009).
[139]Y. Mai and A. Eisenberg, Chem. Soc. Rev. **41**, 5969 (2012).
[140]T. Ghoshal, M. T. Shaw, C. T. Bolger, J. D. Holmes, and M. A. Morris, J. Mater. Chem. **22**, 12083 (2012).
[141]Q. Yang and K. Loos, Polymers **9**, 525 (2017).
[142]J. Xu, J. Varghese, G. Portale, A. Longo, J. Momand, A. Syari'ati, J. A. Heuver, P. Rudolf, B. J. Kooi, B. Noheda, and K. Loos, Polymers **11**, 1598 (2019).
[143]T. Ghoshal, P. G. Fleming, J. D. Holmes, and M. A. Morris, J. Mater. Chem. **22**, 22949 (2012).
[144]B. Yue, X. Jin, P. Zhao, M. Zhu, and L. Zhu, Small **15**, 1804572 (2019).
[145]T. Ghoshal, T. Maity, J. F. Godsell, S. Roy, and M. A. Morris, Adv. Mater. **24**, 2390 (2012).
[146]J. Chai and J. M. Buriak, ACS Nano **2**, 489 (2008).
[147]J. Chai, D. Wang, X. Fan, and J. M. Buriak, Nat. Nanotechnol. **2**, 500 (2007).
[148]W. I. Park, J. M. Yoon, M. Park, J. Lee, S. K. Kim, J. W. Jeong, K. Kim, H. Y. Jeong, S. Jeon, K. S. No, J. Y. Lee, and Y. S. Jung, Nano Lett. **12**, 1235 (2012).
[149]A. Subramanian, G. Doerk, K. Kisslinger, D. H. Yi, R. B. Grubbs, and C.-Y. Nam, Nanoscale **11**, 9533 (2019).

[150]C. Cummins, T. Ghoshal, J. D. Holmes, and M. A. Morris, Adv. Mater. **28**, 5586 (2016).
[151]W. van Zoelen, A. H. G. Vlooswijk, A. Ferri, A.-M. Andringa, B. Noheda, and G. Ten Brinke, Chem. Mater. **21**, 4719 (2009).
[152]J. Varghese, T. Ghoshal, N. Deepak, C. O'Regan, R. W. Whatmore, M. A. Morris, and J. D. Holmes, Chem. Mater. **25**, 1458 (2013).
[153]K. Pandey, K. Ghosh, U. Manna, and M. Biswas, J. Phys. Chem. C **122**, 16325 (2018).
[154]H.-S. Moon, J. Y. Kim, H. M. Jin, W. J. Lee, H. J. Choi, J. H. Mun, Y. J. Choi, S. K. Cha, S. H. Kwon, and S. O. Kim, Adv. Funct. Mater. **24**, 4343 (2014).
[155]L. T. Schelhas, R. A. Farrell, U. Halim, and S. H. Tolbert, Adv. Funct. Mater. **24**, 6956 (2014).
[156]C.-H. Lin, S. Polisetty, L. O'Brien, A. Baruth, M. A. Hillmyer, C. Leighton, and W. L. Gladfelter, ACS Nano **9**, 1379 (2015).
[157]Q. Peng, Y.-C. Tseng, S. B. Darling, and J. W. Elam, Adv. Mater. **22**, 5129 (2010).
[158]D. H. Yi, C.-Y. Nam, G. Doerk, C. T. Black, and R. B. Grubbs, ACS Appl. Polym. Mater. **1**, 672 (2019).
[159]B. K. Barick, A. Simon, I. Weisbord, N. Shomrat, and T. Segal-Peretz, J. Colloid Interface Sci. **557**, 537 (2019).
[160]R. Z. Waldman, D. J. Mandia, A. Yanguas-Gil, A. B. F. Martinson, J. W. Elam, and S. B. Darling, J. Chem. Phys. **151**, 190901 (2019).
[161]Q. Peng, Y.-C. Tseng, S. B. Darling, and J. W. Elam, ACS Nano **5**, 4600 (2011).
[162]D. Berman and E. Shevchenko, J. Mater. Chem. C **8**, 10604 (2020).
[163]R. Azoulay, N. Shomrat, I. Weisbord, G. Atiya, and T. Segal-Peretz, Small **15**, 1904657 (2019).
[164]Y.-C. Tseng, Q. Peng, L. E. Ocola, J. W. Elam, and S. B. Darling, J. Phys.Chem. C **115**, 17725 (2011).
[165]J. Kamcev, D. S. Germack, D. Nykypanchuk, R. B. Grubbs, C.-Y. Nam, and C. T. Black, ACS Nano **7**, 339 (2013).
[166]P. W. Majewski, A. Rahman, C. T. Black, and K. G. Yager, Nat. Commun. **6**, 7448 (2015).
[167]J. Frascaroli, E. Cianci, S. Spiga, G. Seguini, and M. Perego, ACS Appl. Mater. Interfaces **8**, 33933 (2016).
[168]C. Zhou, T. Segal-Peretz, M. E. Oruc, H. S. Suh, G. Wu, and P. F. Nealey, Adv. Funct. Mater. **27**, 1701756 (2017).
[169]R. Z. Waldman, N. Jeon, D. J. Mandia, O. Heinonen, S. B. Darling, and A. B. F. Martinson, Chem. Mater. **31**, 5274 (2019).
[170]T. Ghoshal, T. Maity, R. Senthamaraikannan, M. T. Shaw, P. Carolan, J. D. Holmes, S. Roy, and M. A. Morris, Sci. Rep. **3**, 2772 (2013).
[171]S. Rasappa, T. Ghoshal, D. Borah, R. Senthamaraikannan, J. D. Holmes, and M. A. Morris, Sci. Rep. **5**, 13270 (2015).
[172]R. Lundy, P. Yadav, A. Selkirk, E. Mullen, T. Ghoshal, C. Cummins, and M. A. Morris, Chem. Mater. **31**, 9338 (2019).
[173]T. Ghoshal, J. O'Connell, C. Sinturel, P. Andreazza, J. D. Holmes, and M. A. Morris, Polymer **173**, 197 (2019).
[174]P. S. Chinthamanipeta, Q. Lou, and D. A. Shipp, ACS Nano **5**, 450 (2011).
[175]D. O. Shin, D. H. Lee, H.-S. Moon, S.-J. Jeong, J. Y. Kim, J. H. Mun, H. Cho, S. Park, and S. O. Kim, Adv. Funct. Mater. **21**, 250 (2011).
[176]X. Zu, X. Hu, L. A. Lyon, and Y. Deng, Chem. Commun. **46**, 7927 (2010).
[177]D. H. Kim, S. H. Kim, K. Lavery, and T. P. Russell, Nano Lett. **4**, 1841 (2004).
[178]S. Park, B. Kim, J. Y. Wang, and T. P. Russell, Adv. Mater. **20**, 681 (2008).
[179]D. Borah, S. Rasappa, R. Senthamaraikannan, J. D. Holmes, and M. A. Morris, Langmuir **29**, 8959 (2013).
[180]C. G. Hardy, L. Ren, S. Ma, and C. Tang, Chem. Commun. **49**, 4373 (2013).
[181]S. Park, B. Kim, A. Cirpan, and T. P. Russell, Small **5**, 1343 (2009).
[182]J. Lee, A. K. Mishra, C. Choi, D. Kim, E. Y. Kim, K. Yong, and J. K. Kim, ACS Appl. Mater. Interfaces **12**, 15667 (2020).
[183]A. Subramanian, N. Tiwale, G. Doerk, K. Kisslinger, and C.-Y. Nam, ACS Appl. Mater. Interfaces **12**, 1444 (2020).
[184]C. Cummins, A. Bell, and M. Morris, Nanomaterials **7**, 304 (2017).
[185]C. Sinturel, F. S. Bates, and M. A. Hillmyer, ACS Macro Lett. **4**, 1044 (2015).
[186]M. W. Schulze, C. Sinturel, and M. A. Hillmyer, ACS Macro Lett. **4**, 1027 (2015).
[187]J. Kwak, A. K. Mishra, J. Lee, K. S. Lee, C. Choi, S. Maiti, M. Kim, and J. K. Kim, Macromolecules **50**, 6813 (2017).
[188]Y. Yoshimura, A. Chandra, Y. Nabae, and T. Hayakawa, Soft Matter **15**, 3497 (2019).
[189]S. Donthu, Z. Pan, B. Myers, G. Shekhawat, N. Wu, and V. Dravid, Nano Lett. **5**, 1710 (2005).
[190]Z. Pan, N. Alem, T. Sun, and V. P. Dravid, Nano Lett. **6**, 2344 (2006).
[191]S. Donthu, T. Sun, and V. Dravid, Adv. Mater. **19**, 125 (2007).
[192]S. Donthu, N. Alem, P. Zixiao, L. Shu-You, G. Shekhawat, V. Dravid, K. D. Benkstein, and S. Semancik, IEEE Trans. Nanotechnol. **7**, 338 (2008).
[193]N. Banerjee and S. B. Krupanidhi, J. Alloys Compd. **547**, 147 (2013).
[194]X. Liao, Y.-K. Huang, C. A. Mirkin, and V. P. Dravid, ACS Nano **11**, 4439 (2017).
[195]A. Carretero-Genevrier, J. Gazquez, J. C. Idrobo, J. Oro, J. Arbiol, M. Varela, E. Ferain, J. Rodriguez-Carvajal, T. Puig, N. Mestres, and X. Obradors, J. Am. Chem. Soc. **133**, 4053 (2011).
[196]A. Carretero-Genevrier, N. Mestres, T. Puig, A. Hassini, J. Oró, A. Pomar, F. Sandiumenge, X. Obradors, and E. Ferain, Adv. Mater. **20**, 3672 (2008).
[197]A. Carretero-Genevrier, J. Gázquez, T. Puig, N. Mestres, F. Sandiumenge, X. Obradors, and E. Ferain, Adv. Funct. Mater. **20**, 892 (2010).
[198]A. Carretero-Genevrier, J. Oro-Sole, J. Gazquez, C. Magén, L. Miranda, T. Puig, X. Obradors, E. Ferain, C. Sanchez, J. Rodriguez-Carvajal, and N. Mestres, Chem. Mater. **26**, 1019 (2014).
[199]D. K. Yi, S. J. Yoo, and D.-Y. Kim, Nano Lett. **2**, 1101 (2002).
[200]S.-S. Kim, C. Chun, J.-C. Hong, and D.-Y. Kim, J. Mater. Chem. **16**, 370 (2006).
[201]C. Chen, T. Ding, Z. Qi, W. Zhang, J. Zhang, J. Xu, J. Chen, J. Dai, and C. Chen, Electron. Mater. Lett. **14**, 467 (2018).
[202]M. Banik, P. Chakrabarty, A. Das, S. K. Ray, and R. Mukherjee, Adv. Mater. Interfaces **6**, 1900063 (2019).
[203]C. Li, G. Hong, P. Wang, D. Yu, and L. Qi, Chem. Mater. **21**, 891 (2009).
[204]C. Park, J. Yoon, and E. L. Thomas, Polymer **44**, 6725 (2003).
[205]F. S. Bates, M. A. Hillmyer, T. P. Lodge, C. M. Bates, K. T. Delaney, and G. H. Fredrickson, Science **336**, 434 (2012).
[206]W. Zheng and Z.-G. Wang, Macromolecules **28**, 7215 (1995).
[207]F. S. Bates and G. H. Fredrickson, Phys. Today **52**(2), 32 (1999).
[208]M. Aizawa and J. M. Buriak, J. Am. Chem. Soc. **128**, 5877 (2006).
[209]T. Kubo, R. F. Wang, D. A. Olson, M. Rodwogin, M. A. Hillmyer, and C. Leighton, Appl. Phys. Lett. **93**, 133112 (2008).
[210]M. D. Rodwogin, C. S. Spanjers, C. Leighton, and M. A. Hillmyer, ACS Nano **4**, 725 (2010).
[211]J. G. Son, J. Gwyther, J.-B. Chang, K. K. Berggren, I. Manners, and C. A. Ross, Nano Lett. **11**, 2849 (2011).
[212]J. G. Son, J. Gwyther, J. B. Chang, K. K. Berggren, I. Manners, and C. A. Ross, Nano Lett. **11**, 2849 (2011).
[213]A. K. G. Tavakkoli, S. M. Nicaise, K. R. Gadelrab, A. Alexander-Katz, C. A. Ross, and K. K. Berggren, Nat. Commun. **7**, 10518 (2016).
[214]A. Rahman, P. W. Majewski, G. Doerk, C. T. Black, and K. G. Yager, Nat. Commun. **7**, 13988 (2016).
[215]A. H. Hofman, G. ten Brinke, and K. Loos, Polymer **107**, 343 (2016).